

Towards Robust Neural Image Compression: Adversarial Attack and Model Finetuning

Tong Chen, *Student Member, IEEE*, and Zhan Ma, *Senior Member, IEEE*

Abstract—Deep neural network-based image compression has been extensively studied. However, the model robustness which is crucial to practical application is largely overlooked. We propose to examine the robustness of prevailing learned image compression models by injecting negligible adversarial perturbation into the original source image. Severe distortion in decoded reconstruction reveals the general vulnerability in existing methods regardless of their settings (e.g., network architecture, loss function, quality scale). A variety of defense strategies including geometric self-ensemble based pre-processing, and adversarial training, are investigated against the adversarial attack to improve the model’s robustness. Later the defense efficiency is further exemplified in real-life image recompression case studies. Overall, our methodology is simple, effective, and generalizable, making it attractive for developing robust learned image compression solutions. All materials are made publicly accessible at <https://njuvision.github.io/RobustNIC> for reproducible research.

Index Terms—Neural image compression, model robustness, adversarial attack, adversarial training

I. INTRODUCTION

In the past few years, we have witnessed an exponential growth of deep neural network (DNN) based image coding approaches. These neural network-based image coding (NIC) methods [1]–[10] have emerged with noticeable compression gains over conventional solutions like JPEG [11], JPEG 2000 [12], and even the latest Versatile Video Coding (VVC) based Intra Profile (VVC Intra) [13], promising an encouraging prospects of NIC-based applications and services, particularly for those rate-constrained or bandwidth-limited networked scenarios.

Unprecedented coding gains of aforementioned NIC methods mostly came from the introduction of variational autoencoder (VAE) framework [2], adaptive context modeling in entropy coding [4], attention mechanism [6], [7], etc. It is also worth pointing out that learning-based NIC offered great flexibility for promptly supporting different image sources (e.g., RGB, YUV, Bayer raw image, etc [14]) and loss functions (quality metrics) [15], [16] in task-oriented applications. On the contrary, it requires substantial efforts to enable additional functionalities in traditional image codecs because we have to fully understand the statistical properties of newly-introduced

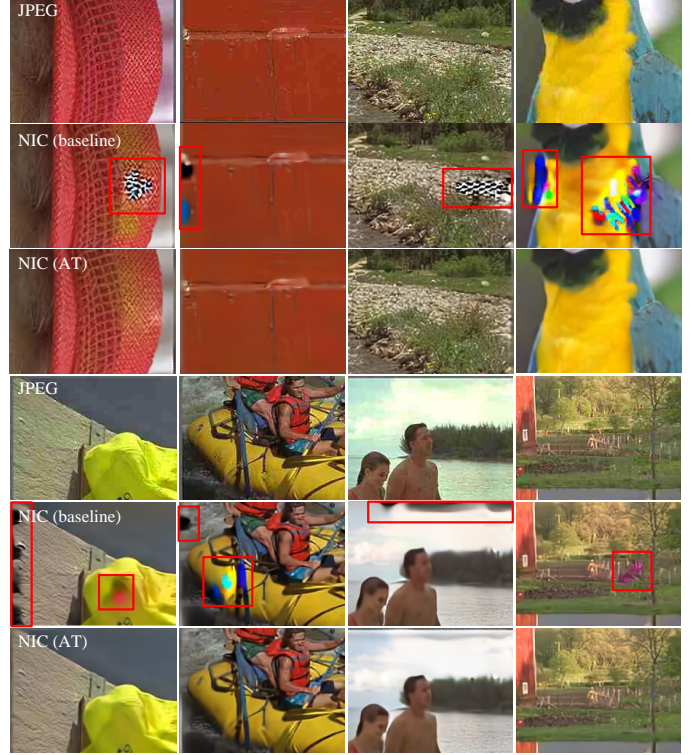


Fig. 1: **Image Recompression.** Row-wisely visual comparison of image reconstructions after being repetitively compressed 50 times using the JPEG (<http://libjpeg.sourceforge.net/>), a pretrained NIC baseline model (Ballé2018 [2]) is used as an example), and an adversarially retrained Ballé2018 model, referred to as NIC (AT). More details can be found in Sec. V.

image sources and optimization metrics to develop effective coding toolkits. For example, it takes several years to facilitate the efficient compression of screen content sources when standardizing the extensions of High-Efficiency Video Coding (HEVC) [17].

Recently, after serial exploration studies, the ISO/IEC JPEG (Joint Photographic Experts Group) committee has made concrete progress on the performance and complexity evaluation of various NIC solutions and is now standardizing the next-generation image codec using deep learning techniques. Besides the superior compression efficiency, model robustness/generalization is yet another critical factor for the potential success of such learned approaches, which is often overlooked and not thoroughly examined in the past.

Observation and Motivation. We first present a real-life

This work was partially supported by the National Natural Science Foundation of China under Grant 62022038.

Copyright © 2023 IEEE. Personal use of this material is permitted. However, permission to use this material for any other purposes must be obtained from the IEEE by sending an email to pubs-permissions@ieee.org.

T. Chen and Z. Ma are with the School of Electronic Science and Engineering, Nanjing University, Nanjing, Jiangsu, 210093 China. E-mails: tong@smail.nju.edu.cn, mazhan@nju.edu.cn. (Corresponding Author: Z. Ma)

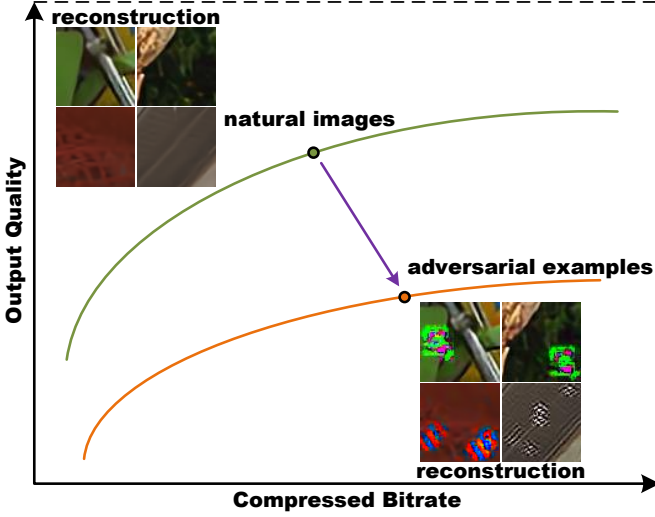


Fig. 2: **Impact of adversarial attack in image compression.** Adversarial examples are generated to test whether the overall coding performance of NIC models would be affected.

application example in Fig. 1. As seen, unexpected pixel impairments are observed if the image is compressed multiple times using learned approaches, while similar phenomena are not detected in images re-compressed using rules-based conventional methods like JPEG. Such iterative or successive compression is a common practice for image-based applications over the Internet where images may be re-edited, re-compressed, and re-distributed often. Similar observations are also reported by Kim *et. al* in [18].

Nevertheless, such instability may not be solely in image recompression scenarios [18]. A systematic stability and generalization study of popular VAE-based compression models on full-resolution images still remains untouched and is urgently needed for the pursuit of robust NIC methods because the signal fidelity of image reconstruction plays a vital role in vast applications such as medical imaging, autonomous self-driving, face recognition, security surveillance, etc. For instance, having incorrect (unexpected) spatial textures in decoded images may lead to very different outcomes of specific tasks (e.g., image classification) [19] (see Fig. 24 and Fig. 25 in the supplemental material), or may also present annoying/disturbing artifacts [18] with severely-degraded user experience (see Fig. 9).

Technically, an image compression network sometimes might be roughly categorized as one type of image-to-image task model. However, we would like to note that there are fundamental differences between image compression and popular image-to-image tasks. A typical image-to-image processing task mainly optimizes the distance (distortion) between the output target and ground truth, while image compression deals with the rate and distortion jointly.

Generally, an image compression network separates the encoder and decoder, and applies the quantization upon the activation elements at the bottleneck layer for rate-distortion optimization. Various quantization levels would affect the sparsity of the latent representation and finally result in different

quality scales (or target bitrates). As illustrated in Fig. 2, we try to generate adversarial examples by adding negligible perturbation into the original source images, but the compression of adversarial examples would lead to severe distortion in decoded reconstruction. As seen, the robustness of an image compression algorithm has affected the reconstruction quality and compression bitrate jointly.

All of these thus make the robustness analysis of existing image compression networks an issue worthy of a separate and in-depth study.

Approach. Unfortunately, it is almost impossible to manually search for all potential cases that may cause model instability and deteriorate performance. As inspired by recent adversarial attack studies on high-level vision tasks [20]–[24] and low-level image-to-image tasks [25]–[27] to respectively examine their model robustness, we suggest implementing the adversarial attack to analyze and characterize its impacts on the robustness and coding efficiency of the underlying NIC models, quantitatively and qualitatively.

Later we extensively explore possible defense strategies and their effects on the robustness improvement of NIC methods to adversarial attacks. An implementation of our defense strategy in practical application is also exemplified. As shown in Fig. 1 and Fig. 19, the proposed defense strategies can effectively eliminate the distortions induced by image recompression.

Contributions.

- 1) To the best of our knowledge, this is the first work that performs the adversarial attack to systematically study the model robustness of learned image compression on full resolution images (Sec. III); Different from most existing works that mainly qualitatively evaluate the attack and defense methods, we propose a metric – Δ PSNR for quantitative analysis which is shown to be effective in experiments.
- 2) Our extensive experiments report the general vulnerability of existing learning-based image compression methods regardless of the underlying model settings and the perturbation generation strategy (Sec. IV); A novel Fast Threshold-constrained Distortion Attack (FTDA) approach is proposed to generate adversarial examples with balanced performance and complexity while existing methods like CW [28] or I-FGSM [29] mostly satisfy one aspect, i.e., performance or complexity.
- 3) We further improve the model’s robustness against attacks through the use of various defense strategies including geometric self-ensemble, adversarial training as well as image pre-processing techniques like spatial re-sizing and bit depth reduction. Their impact on compression efficiency is thoroughly examined and discussed (Sec. V). As a result, adversarial training and geometric self-ensemble are suggested because of their convincing efficiency, while spatial resizing or bit depth reduction induced pre-processing distortion inherently deteriorates the performance of the underlying compression model which is not acceptable for applications.

Overall, our methodology which includes the adversarial example generation and the defense strategies for improving the model robustness is simple, effective, and generalizable

to popular learned image compression approaches, making it attractive and necessarily desired for practical application.

II. RELATED WORKS

This section briefs relevant techniques on respective lossy image compression and adversarial attack.

A. Lossy Image Compression

Lossy image compression approaches like JPEG [11], JPEG 2000 [12], VVC Intra [13], etc, search for appropriate compact representation through rate-distortion optimization (RDO). Typically, they adopt the “transform coding” or “hybrid transform/prediction coding” to transform input pixels, or pixel residuals (after intra prediction) into frequency domain coefficients for quantization and entropy coding. These transforms are generally comprised of a set of basis functions that are weighted to represent arbitrary pixel-domain blocks/patches using a few sparse, nonzero coefficients.

Classical Methods. Classical transforms include Discrete Cosine Transform (DCT) [33], Wavelet Transform [34], and so on. Taking DCT as an example, transformed coefficients are usually clustered at a few low-frequency positions which can be leveraged for energy compaction. The DCT is invertible, i.e., the original image \mathbf{x} can be reconstructed losslessly by applying the inverse DCT (IDCT), e.g., $\mathbf{x} = f_{\text{dct}}^{-1}(f_{\text{dct}}(\mathbf{x}))$. Here f_{dct} and f_{dct}^{-1} are DCT and IDCT respectively.

Over-complete Dictionary. Image data typically exhibit non-stationary behavior, making it difficult to be de-correlated sufficiently by existing DCT or wavelets. Dictionary learning is then introduced to use a number of content-adaptive, over-complete dictionary atoms to represent image blocks using more sparse and easy-to-compress coefficients [35], [36].

Neural Transform. Built upon the excessive representation capacity of high-dimensional data, deeply stacked convolutional neural networks (CNNs) are therefore utilized to construct neural transforms to represent image blocks in a more compact means (see Fig. 3b). Figure 3a plots a popular VAE architecture that applies neural transform and demonstrates superior coding efficiency [1], [2], [4], [6], [7], [37].

The forward transform in the encoder analyzes the original image source \mathbf{x} and represents it using compact, vectorized latent features \mathbf{z} for quantization (e.g., $\hat{\mathbf{z}} = \mathbf{Q}(\mathbf{z})$) and entropy coding with learned adaptive contexts. Oppositely, the backward transform in the decoder mirrors the forward steps in the encoding process to generate the reconstruction $\hat{\mathbf{x}}$. As usual, the RDO module controls the compression trade-off by a hyperparameter λ , e.g.,

$$R + \lambda D = \underbrace{\mathbb{E}[-\log_2 p(\hat{\mathbf{z}})]}_{\text{rate}} + \lambda \underbrace{\mathbb{E}[\|\mathbf{x} - \hat{\mathbf{x}}\|_2^2]}_{\text{distortion}}. \quad (1)$$

with $p(\hat{\mathbf{z}})$ standing for the estimated probability of feature elements at the bottleneck layer [7].

Unlike DCT or wavelet transform, the neural transforms $f_E()$ in the encoder and $f_D()$ in the decoder are usually non-linear functions. Although formally the encoder and decoder are of symmetrical structure, their coefficients are independently random-initialized and then optimized by specific

TABLE I: Quality Scales

Quality	1	2	3	4	5	6
MSE	0.0018	0.0035	0.0067	0.0130	0.0250	0.0483
MS-SSIM	2.40	4.58	8.73	16.64	31.73	60.50

stochastic gradient descent algorithms, thus their invertibility is not mathematically guaranteed even without quantization error, i.e.,

$$\mathbf{x} \neq f_D(f_E(\mathbf{x})). \quad (2)$$

Even having invertible neural transform as studied in [38], [39], the quantization error in lossy compression may also be amplified during the layer-by-layer decoding process. For either case, $f_D()$ and $f_E()$ are made up of a stack of convolutional layers that consist of linear convolution, non-linear activation, and optional spatial re-sampling, with which it would potentially amplify specific perturbation through layer-by-layer computation and finally lead to unexpected impairments.

As explained in previous works [20], [40], nonlinear neural networks are still too linear to resist linear adversarial perturbation. By iteratively updating the adversarial perturbation with smaller steps, linear adversarial perturbation in high-dimensional spaces is sufficient to cause the vulnerability issue of underlying deep neural networks. A successful attack to image-to-image networks also implies that deep neural transform based NIC methods are potentially vulnerable to adversarial perturbation.

B. Adversarial Attack and Defense

Attack. Adversarial attacks have been widely utilized to evaluate the robustness of DNN models in various approaches, particularly for those high-level vision tasks as aforementioned. As known, these DNN models basically wish to construct a non-linear mapping function g to effectively characterize the relationships between input data and output results.

An adversarial attack can be either *targeted* or *untargeted*. Given a vectorized input \mathbf{x} and a mapping function $y = g(\mathbf{x})$, for an *untargeted* attack, adversarial examples \mathbf{x}^* are used to produce undesigned but incorrect output. They can be derived using:

$$\underset{\mathbf{x}^*}{\operatorname{argmin}} d\{\mathbf{x}, \mathbf{x}^*\} \text{ s.t. } g(\mathbf{x}^*) \neq g(\mathbf{x}). \quad (3)$$

Here $d\{\cdot\}$ measures the signal distance between original \mathbf{x} and adversarial example \mathbf{x}^* , for which conventional MSE or other metrics can be used.

The adversarial attack can be also *targeted*. Taking image classification as an example, a targeted attack, as the name implies, attempts to use example \mathbf{x}^* that has limited perturbation compared with original input \mathbf{x} , to “fool” the classifier f to misclassify \mathbf{x}^* to some targeted label $y^t = f(\mathbf{x}^*)$ that is different from the original outcome y . Such targeted adversarial examples can be generated through:

$$\underset{\mathbf{x}^*}{\operatorname{argmin}} d\{\mathbf{x}, \mathbf{x}^*\} \text{ s.t. } f(\mathbf{x}^*) = y^t. \quad (4)$$

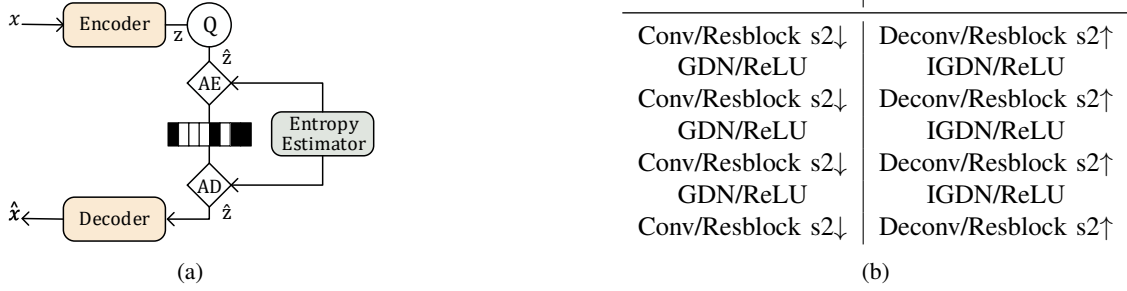


Fig. 3: **Neural Image Compression (NIC)**. (a) Basic architecture of VAE-based NIC Solutions. Q denotes the quantization. The entropy estimator provides the probability estimation for both AE (Arithmetic Encoding) and AD (Arithmetic Decoding); x is the input source image, and correspondingly \hat{x} is the output reconstruction (after decoding). (b) Typical paired Encoder and Decoder components used in NIC framework, such as normal Convolutional layer (Conv) or ResNet block (Resblock) [30], resolution re-sampling (upsampling $s2\uparrow$ and downsampling $s2\downarrow$ at a factor of 2), nonlinear activations using GDN (Generalized Divisive Normalization) [31] or ReLU (rectified linear unit) [32]. Deconv and IGDN are inverted processes of respective Conv and GDN.

TABLE II: Tested NIC Approaches and Their Key Components.

Methods	Key Components		
	Nonlinear Transform	Entropy Model	Loss
Ballé 2016 [1]	Conv+GDN	factorized	MSE / MS-SSIM
Ballé 2018 [2]	Conv+GDN	hyperprior	MSE / MS-SSIM
Minnen [4]	Conv+GDN	joint hyperprior & autoregressive	MSE
Cheng 2020 [6]	Resblock+Spatial-Channel Attention	joint hyperprior & autoregressive	MSE
NLAIC [7]	Resblock+Nonlocal Attention	joint hyperprior & autoregressive	MS-SSIM
HiFiC [5]	Conv+Channel Normalization	hyperprior	MSE + LPIPS [41] + GAN
Weixin 2021 [42]	Fixed-point NLAIC	joint hyperprior & autoregressive	MSE
InvCompress [39]	INN+Attention+Feature Enhancement	joint hyperprior & autoregressive	MSE

It was first observed in [43] that deep neural networks are vulnerable to adversarial perturbation. Since then, researchers have further explored several attack strategies [20], [28], [29], [40], [44], [45] for generating adversarial examples. Fast gradient-based techniques like FGSM [20] used the sign of gradient to generate a coarse approximation of optimal examples in one step. Further, I-FGSM [29] extended the FGSM method by iterating the process with a smaller step size to improve the attack performance. Later, I-FGSM was further refined with multiple random starts in [46] (PGD), or with momentum item in [47] (MI-FGSM). However, our experiments revealed almost negligible differences among I-FGSM, PGD, and MI-FGSM regarding the attack performance quantitatively measured by the proposed Δ PSNR. Thus, we mainly use I-FGSM for comparative study in the paper. Carlini and Wagner [28] then introduced a more effective algorithm (referred to as CW) to best guarantee a successful attack with minimal perturbation injected. The CW method can be formulated under l_0 , l_2 , l_∞ norms, and is able to take advantage of modern optimizers such as Adam [48] to generate adversarial examples for the attack.

Defense. To deal with the threat caused by adversarial attacks, many defense techniques have also been proposed. Pre-processing based approaches like JPEG compression [49], random resizing [50], bit depth reduction [51] and geometric self ensemble [52] attempt to pre-process the input image to eliminate the effects caused by perturbations. Another very effective way of defense is adversarial training that augments

adversarial examples in training set [20], [21], [29], [53]–[55] to directly improve the robustness of the underlying learned model for various vision tasks.

Existing attempts of adversarial attacks on VAE-based methods [56], [57] only focus on generative models like VAE-GAN [58] and mainly use very low-resolution (e.g. 28×28), simple digital number datasets like MNIST and SVHN [59]. To the best of our knowledge, there has been no existing work on attacking full-resolution image compression frameworks. As aforementioned, the stability of decoded reconstruction in image compression tasks is critical to vast applications. Therefore, in this paper, we will first demonstrate how existing image compression models are affected by the untargeted attack and then show how to defend them for robust image compression.

Robustness Evaluation. Most previous works have focused on attacking computer vision systems. Therefore, they generally use the performance drop in their corresponding tasks (e.g., classification accuracy in classification tasks) to evaluate the attack performance. For adversarial attacks in image-to-image tasks (super-resolution [25], [27], [60], optical flow [26], denoising/deblurring [27], etc.), attack performance is often evaluated by qualitatively showing visual examples together with some objective metric results. To better evaluate the vulnerability of a given image compression model, a proper metric is highly desired to measure and compare the degree of vulnerability quantitatively. In this case, we propose the Δ PSNR metric to quantify them effectively.

III. ADVERSARIAL EXAMPLES

Images are mostly compressed for vast applications due to rate/bandwidth constraints in practice. The compression technology behind is mandated to guarantee interoperability across heterogeneous platforms, client devices, etc, which is often presented as an international standard or industrial recommendation that is reproducible and publicly accessible. Hence, we generally assume that the attacker can have full access to the NIC codec and model parameters to best generate adversarial examples for attacks [57]. As a result, technically the proposed attack strategies belong to *white-box* attack. Besides, such an adversarial attack is referred to as the “untargeted” attack without a designated purpose that particularly aims for misleading the semantic understanding of the reconstructed content. In the companion supplemental material, we also demonstrate how a targeted attack can affect the outcome of NIC methods.

Without making any modification to the parameters of pretrained encoder $f_E()$ and decoder $f_D()$ of a specific NIC method, the attacker wishes to inject perturbation \mathbf{n} upon the original source image \mathbf{x} to generate the adversarial example $\mathbf{x}^* = \mathbf{x} + \mathbf{n}$. These images are respectively encoded and decoded to have the original reconstruction $\hat{\mathbf{x}} = f_D(f_E(\mathbf{x}))$, and the adversarial $\hat{\mathbf{x}}^* = f_D(f_E(\mathbf{x}^*))$. Both \mathbf{x}^* and $\hat{\mathbf{x}}^*$ are constrained in the range of $[0, 1]$. The generated \mathbf{x}^* shall present negligible perturbation compared with the original input \mathbf{x} , while the decoded adversarial reconstruction $\hat{\mathbf{x}}^*$ is expected to largely differ from the original reconstruction $\hat{\mathbf{x}}$ with visible distortion. Therefore, the adversarial examples for such untargeted distortion attacks can be formally defined as follows:

$$\begin{aligned} & \text{maximize} \quad \mathcal{D}(\hat{\mathbf{x}}, \hat{\mathbf{x}}^*) \\ & \text{s.t.} \quad \mathcal{D}(\mathbf{x}, \mathbf{x}^*) < \epsilon, \\ & \quad \mathbf{x}^*, \hat{\mathbf{x}}^* \in [0, 1]. \end{aligned} \quad (5)$$

Here \mathcal{D} is the distance metric that can be the MSE or MS-SSIM, and ϵ is the threshold used to control the input perturbation.

Fast Threshold-constrained Distortion Attack (FTDA). To solve (5), we proposed the FTDA to optimize the adversarial example generation:

$$\arg \min_{\mathbf{n}} L_d = \begin{cases} \frac{\|\mathbf{n}\|_2^2}{N}, & \frac{\|\mathbf{n}\|_2^2}{N} \geq \epsilon, \\ 1 - \frac{\|\hat{\mathbf{x}} - \hat{\mathbf{x}}^*\|_2^2}{N}, & \frac{\|\mathbf{n}\|_2^2}{N} < \epsilon. \end{cases} \quad (6)$$

where ϵ is the l_2 threshold and N is the total num of image pixels. In this paper, we mainly use l_2 distance for \mathcal{D} because l_2 related PSNR metric is widely used for image compression quality measurement. We also show some examples in Fig. 20 in the supplemental material that other distance metrics, such as the l_1 distance and MS-SSIM [15], can be used to guide the example generation.

Equation (6) is a piecewise function. When augmented noise is strong, e.g., $\frac{\|\mathbf{n}\|_2^2}{N} \geq \epsilon$, the objective function is first to decrease the noise intensity until $\frac{\|\mathbf{n}\|_2^2}{N} < \epsilon$; hereafter, we use the negative l_2 distance between the original reconstruction $\hat{\mathbf{x}}$ and adversarial reconstruction $\hat{\mathbf{x}}^*$ to maximize their distance. The threshold ϵ can enforce the same level of perturbation

added in the input and maximize the output distortion in the meantime. We can easily adapt ϵ to get proper adversarial examples as expected. The proposed perturbation generation strategy in (6) is a general approach that is effective for any NIC models used in practice. As will be shown in Sec. V, these generated adversarial examples can be used to retrain existing NIC models and effectively mitigate the artifacts induced by adversarial attacks and successive image compression.

Besides, existing attack approaches can also be extended to solve (5), where certain adjustments are implemented to adapt them for the untargeted distortion attack. Here we choose commonly used I-FGSM [29] and CW- l_2 [28] for evaluation in the following section.

I-FGSM. Here is the optimization function used for I-FGSM. $\text{sgn}()$ is a sign function applied to the backpropagated gradient. At the i -th step,

$$\mathbf{x}_{(i+1)}^* = \mathbf{x}_{(i)}^* + \frac{\epsilon}{T} \text{sgn} \left(\nabla \left\| \hat{\mathbf{x}}_{(i)}^* - \hat{\mathbf{x}} \right\|_2 \right). \quad (7)$$

Similar to (6), here ϵ also controls the level of input perturbation. T is the iterations needed for example generation which is set to 16 in default.

CW- l_2 . The original version of the CW attack was designed for the targeted attack as:

$$\begin{aligned} & \text{minimize} \quad \|\delta\|_p + c \cdot f(x + \delta), \\ & \text{such that} \quad x + \delta \in [0, 1]. \end{aligned} \quad (8)$$

where $\|\delta\|_p$ is the l_p norm of perturbation δ and $f(x + \delta)$ is predefined objective function. For a fair comparison, the l_2 norm is used in our experiments and the negative l_2 distance is applied as the objective function. The final adjusted CW- l_2 used in this work is formulated as:

$$\begin{aligned} & \text{minimize} \quad \frac{\|\mathbf{n}\|_2^2}{N} + \left(1 - c \cdot \frac{\|\hat{\mathbf{x}}^* - \mathbf{x}\|_2^2}{N} \right), \\ & \text{such that} \quad \hat{\mathbf{x}}^*, \mathbf{x}^* \in [0, 1]. \end{aligned} \quad (9)$$

Here c is a constant that needs to be suitably chosen. In order to achieve the optimal attack performance and also control the input perturbation level, we use a binary search strategy to find the optimal c following the implementation suggested by the authors of the original CW method [28]. For each c under consideration, we run 1000 iterations in default to minimize (9) with the Adam optimizer.

IV. ATTACK EVALUATION

A. Δ PSNR

Recalling the attack formulation in (5), we hope the negligible perturbation at the input would bring severe distortion to the output, which implies that the underlying network enlarges the input perturbation through layer-wise computation. In this case, we suggest measuring the vulnerability by the level of the perturbation amplification. Therefore, a Δ PSNR is used:

$$\begin{aligned} \Delta \text{PSNR} = & \\ & -10 \log_{10} \frac{\|\mathbf{x}^* - \mathbf{x}\|_2^2}{\|\hat{\mathbf{x}}^* - \hat{\mathbf{x}}\|_2^2} = \text{PSNR}_{\text{in}} - \text{PSNR}_{\text{out}}. \end{aligned} \quad (10)$$

Δ PSNR means the quality degradation measured by PSNR. As seen, $\Delta \text{PSNR} > 0$ means that the input perturbation is

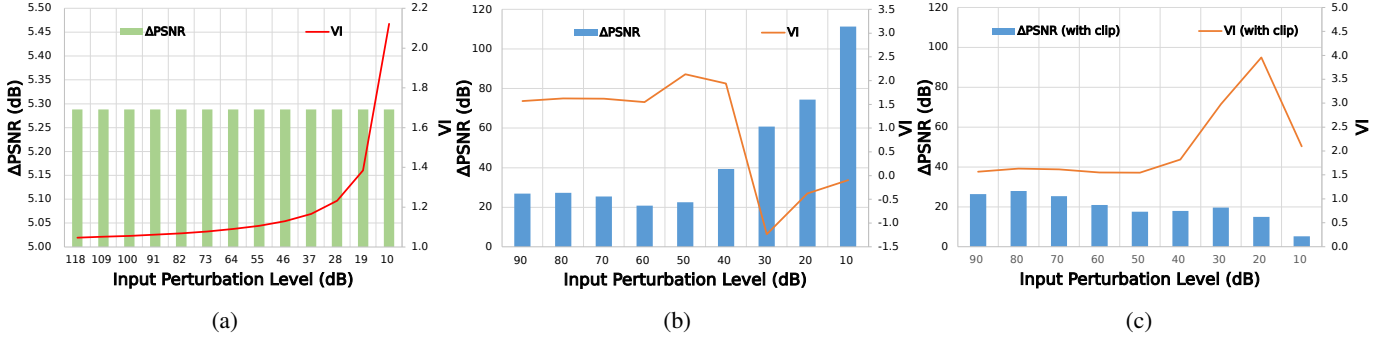


Fig. 4: Vulnerability metric comparison. ΔPSNR can better represent the quality degradation at various input perturbation levels controlled by ϵ in (6). Kodak images are used in this example. (a) A toy linear network using one-layer convolution for both encoder and decoder; (b) non-linear NIC; (c) NIC with clipping to ensure $\mathbf{x}^*, \hat{\mathbf{x}}^* \in [0, 1]$ as in (5). For (b) and (c), A pretrained Ballé2018 model is tested.

magnified by the network so the output distortion is larger than the input perturbation, while $\Delta\text{PSNR} < 0$ means that the input perturbation is suppressed to a smaller level.

Alternatively, a Vulnerability Index (VI) metric was used in [27] for evaluating the vulnerability of image processing networks. It is calculated as the PSNR ratio between the input and output:

$$\text{VI} = \frac{-10 \log_{10} \|\mathbf{x}^* - \mathbf{x}\|_2^2}{-10 \log_{10} \|\hat{\mathbf{x}}^* - \hat{\mathbf{x}}\|_2^2} = \text{PSNR}_{\text{in}} / \text{PSNR}_{\text{out}}. \quad (11)$$

Figure 4 provides a comparison of these two measurements. For a tested model with fixed parameters, the VI metric shows obvious sensitivity to the absolute level of input perturbation even for linear networks as in Fig. 4a. However, the magnification level presented by ΔPSNR is more stable across different perturbation levels. As a result, the ΔPSNR is a preferred metric to measure the intrinsic vulnerability of an image compression model without being biased by the absolute magnitude of input perturbation. More details are given in the supplemental material.

In the following sections, ΔPSNR will be used for performance evaluation. For measuring the attack performance, higher ΔPSNR means better attack performance; while for the defense efficiency, lower ΔPSNR indicates better defense efficiency.

B. Channel-wise Activation Variation (CAV)

Besides, we offer another perspective by visualizing and comparing the channel-wise activation in latent feature space. As shown in Fig. 5, the **safe zone** indicates the range of activation magnitudes counted over 10,000 training images. The activation intensity of the original natural image (without noise injection) is very likely to stay within this region. However, for the activation intensity of adversarial examples, noticeable outliers are observed, especially for some channels that are much less activated by natural images. Such qualitative visualization of CAV well supplements the objective ΔPSNR . Having them together provides a comprehensive evaluation to study the impact of the adversarial attack on image compression models.

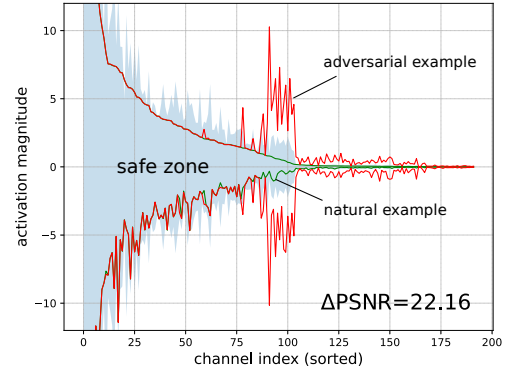


Fig. 5: **Channel-wise Activation Variation (CAV)**. The range of channel-wise activation magnitude at the bottleneck layer for the original natural image and its corresponding adversarial example is illustrated. The channels are sorted in descending order according to the range of activation magnitude of the original natural image. An MS-SSIM optimized Ballé2018 model is exemplified.

C. Adversarial Example Generation Settings

In order to find optimal settings for adversarial example generation, a variety of experiments are conducted first.

1) *Attack Strategy Comparison*: Figure 6 presents the attack performance of I-FGSM, $\text{CW-}l_2$, and the proposed FTDA (Ours). As a comparative anchor, we also provide the PSNR degradation caused by random noise attack and blurry degradation. As you can observe, compression networks tend to suppress the effect of random noise but dramatically amplify the adversarial perturbation generated by other attack methods. Among them, the $\text{CW-}l_2$ algorithm shows slightly better performance than our proposed method measuring by ΔPSNR .

In addition to the attack performance, computational complexity is another vital factor for the successful adoption of a potential attack strategy. Therefore, when comparing different attack methods, we also take the computational complexity (measured by the time duration in seconds for example generation) into consideration.

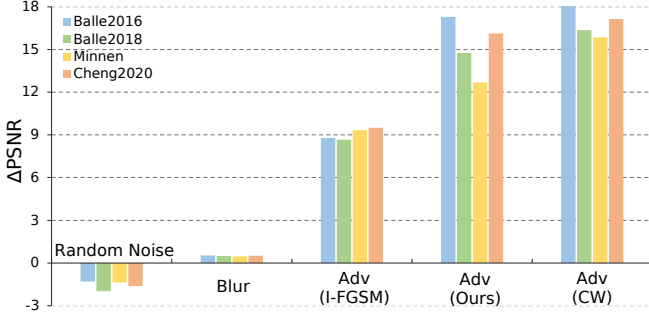


Fig. 6: **Attack performance of different strategies measured by Δ PSNR.** The input perturbation is controlled at the same level of $1e-4$ for different methods including the gaussian random noise and blur. Results for each method are averaged over all quality scales and metrics in Table I on Kodak images.

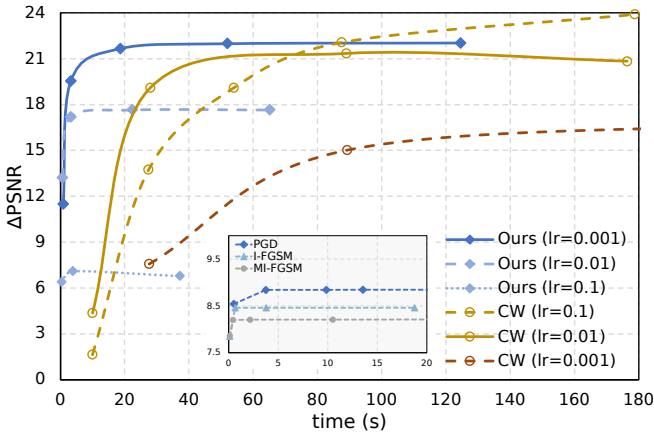


Fig. 7: **Attack performance vs. complexity for different attack strategies.** A pretrained Ballé2018 model is used here as an example. Various learning rates at 0.001, 0.01, and 0.1 are tested for CW and the proposed method. For each learning rate, binary search steps are modified accordingly to obtain the CW performance at different time complexities. Our proposed method performs better when having complexity limitations, while the CW can achieve better performance with much higher computational complexity. Three FGSM-based methods (I-FGSM, MI-FGSM and PGD) show very close Δ PSNR (e.g., between 8 and 9).

The results are illustrated in Fig. 7. As mentioned earlier, I-FGSM is very fast because of its gradient sign computation. But the coarse adversarial examples it generates are less effective with the least Δ PSNR (see the subplot embedded). The CW- l_2 in (9) needs to search for the best c in order to get optimal adversarial attack performance. The searching process inevitably leads to much higher computational complexity. If setting no computational complexity constraint for all strategies, the CW- l_2 can reach at the best attack performance. However, it is impractical to use the CW- l_2 for large-scale adversarial example generation and subsequent adversarial training. In this case, our proposed FTDA finds a justified balance between complexity and performance.



Fig. 8: **Impact of input perturbation level ϵ .** Illustration of adversarial examples at the first row, associated perturbation at the second row, and corresponding decoded reconstructions at the third row for different perturbation levels. ϵ is adjusted to adapt the intensity of input perturbation, i.e., larger ϵ indicates stronger perturbation. Both Δ PSNR and VI are presented. Still here VI always tends to increase with the absolute perturbation level.

2) *Perturbation Level ϵ :* Figure 8 further visualizes adversarial examples when having different levels of input perturbation adapted by the ϵ . The results are consistent with the intuition, i.e., larger ϵ leads to stronger noise for the input image, and thus yields more severely-degraded reconstructions. Surprisingly, even with negligible visual artifacts when $\epsilon = 1e-5$, impaired pixels are still presented in decoded reconstruction, implying the general vulnerability of NIC models. As also observed in Fig. 8, the input perturbation would become visible when ϵ is increased to $1e-3$. To control the input perturbation basically imperceptible, the default noise threshold ϵ in (6) is set to $1e-4$ for the following experiments, having the PSNR between the original natural image and corresponding adversarial example equal to 40 dB.

D. Evaluation on NICs

Experiments in the previous section have shown some preliminary evidence that existing NIC models are vulnerable to adversarial attacks. In this section, we will perform more tests and further explore the influence of different NIC settings on the model vulnerability.

1) *General Observation:* We choose a variety of VAE-based NICs listed in Table II to demonstrate the general existence of vulnerability issue among these recently emerged

solutions. These NICs exemplify major milestones during the development of learning-based image coding.

Theoretically, image coding efficiency is highly related to the efficiency of nonlinear transform and entropy context modeling. Earlier attempts made in Ballé2016 [1] first introduced the GDN (Generalized Divisive Normalization) with convolutional layers and applied a simple factorized entropy model that was further improved in Ballé2018 [2] and Minnen [4] by hyperprior, and joint hyperprior and autoregressive neighbors for better entropy modeling; Because of the superior efficiency by using joint hyper prior and autoregressive neighbors, succeeding works almost reused the same mechanism in context modeling.

Given that convolution is calculated using equal weights at all spatial locations, Cheng2020 [6] and NLAIC [7] suggested the attention mechanism to aggregate local or nonlocal correlations to enhance the performance. Previous discussions mainly applied the MSE or MS-SSIM as the loss function in training while HiFiC [5] combined the MSE, LPIPS (Learned Perceptual Image Patch Similarity), and GAN (Generative Adversarial Network) loss to noticeably improve the perceptual quality of reconstructed images.

In addition to the coding efficiency, other aspects were considered as well. For example, the aforementioned models with floating point computation were platform-dependent and complexity intensive. In Weixin2021 [42], it developed the fixed point strategy to optimize the NLAIC [7], yielding negligible performance loss but significant complexity reduction. Note that nonlinear transforms in [1], [2], [4], [6], [7] were not invertible and could not avoid the information loss, the InvCompress [39] used invertible neural network (INN) as its core transform to resolve this issue.

We generally utilize open-source code and pretrained models of these methods (e.g., compressAI¹ [61], NLAIC², Weixin2021³, HiFiC⁴ and InvCompress⁵) to avoid any ambiguity and inconsistency. For those missing models, we strictly follow the training procedures to reproduce them from scratch. The hyperparameter λ s used for different quality scales follow the setting provided by CompressAI as listed in Table I. For a fair comparison, we run 1k steps with a learning rate at 0.01 with three times learning rate decay and noise threshold ϵ at $1e-4$ to generate adversarial examples for each NIC method listed in Table II using images from Kodak dataset [62]. Adam [48] optimizer is used to optimize the (6).

In Fig. 9, the adversarial inputs and corresponding reconstructions are visualized for multiple methods⁶. Visible impairments are clearly presented in these reconstructions. Quantitative results in Table III with significant PSNR degradation (e.g., > 10 dB) also confirm the subjective loss, implying the general vulnerability issue in prevalent learning-based image coding frameworks regardless of their transforms,

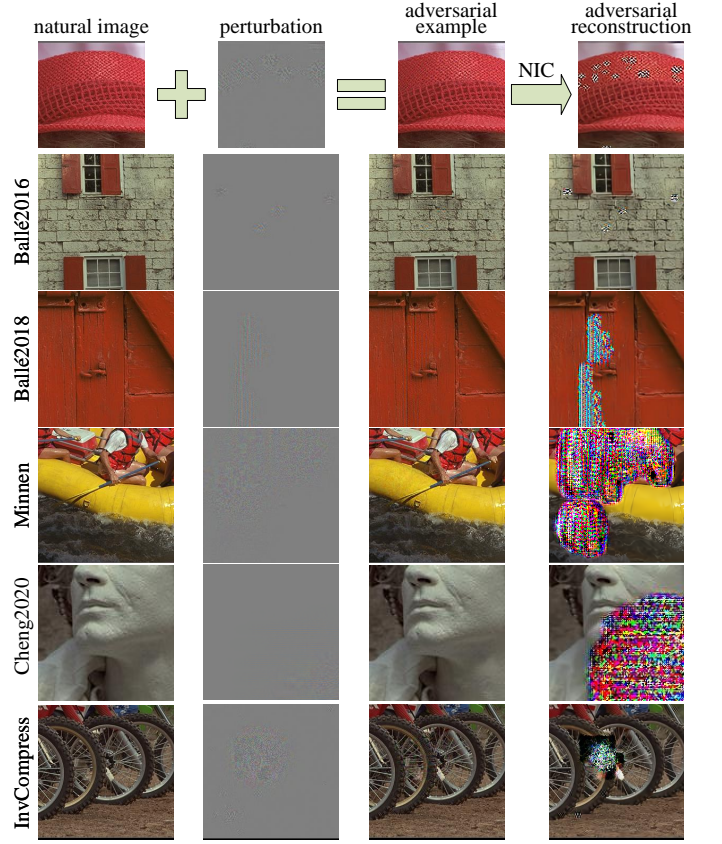


Fig. 9: **Examples of Model Vulnerability Incurred Reconstruction Distortions.** More quantitative comparisons between different methods can be found in Table III.

entropy models, and optimization methods utilized (see more details in Table II). Even for InvCompress [39] that applied a quite different invertible neural network to avoid information loss, the model vulnerability is still presented with obvious distortion in Fig. 9, which might be caused by the use of (non-linear) feature enhancement modules before and after the invertible neural network transforms.

TABLE III: The bitrate increase (Δ bpp) and Δ PSNR of adversarial examples ($\epsilon=1e-4$) compared with original images averaged on Kodak dataset across all 6 quality levels (except for HiFiC, which only has 3 available pretrained levels). The “mse” and “ms-ssim” indicate the MSE and MS-SSIM optimized model respectively.

Methods	Metrics	bpp (ori)	bpp (adv)	Δ bpp	Δ PSNR
Ballé2016	mse	0.4415	0.4578	+3.69%	14.03
	ms-ssim	0.3443	0.3642	+5.78%	20.55
Ballé2018	mse	0.4569	0.5044	+10.40%	11.38
	ms-ssim	0.3301	0.3686	+8.80%	16.45
Minnen	mse	0.4234	0.4636	+9.49%	10.39
	ms-ssim	0.3136	0.3494	+11.42%	14.96
Cheng2020	mse	0.3966	0.8467	+113.49%	18.27
	ms-ssim	0.3050	0.3425	+12.30%	13.98
InvCompress	mse	0.2967	0.3160	+6.50%	13.03
NLAIC	mse	0.4144	0.4748	+17.79%	10.22
	ms-ssim	0.3348	0.3622	+8.17%	15.00
Weixin2021	mse	0.3174	0.3319	+4.56%	11.54
HiFiC	LPIPS	0.2574	0.2679	+4.08%	13.51

¹<https://github.com/InterDigitalInc/CompressAI>

²<https://njuvision.github.io/NIC/>

³<https://njuvision.github.io/fixed-point/>

⁴<https://github.com/tensorflow/compression/tree/master/models/hific>

⁵<https://github.com/xyq7/InvCompress>

⁶We use different images for diverse NIC solutions to exemplify the severe quality degradation of decoded images incurred by the model vulnerability. Such visible distortions are presented for other images as well.

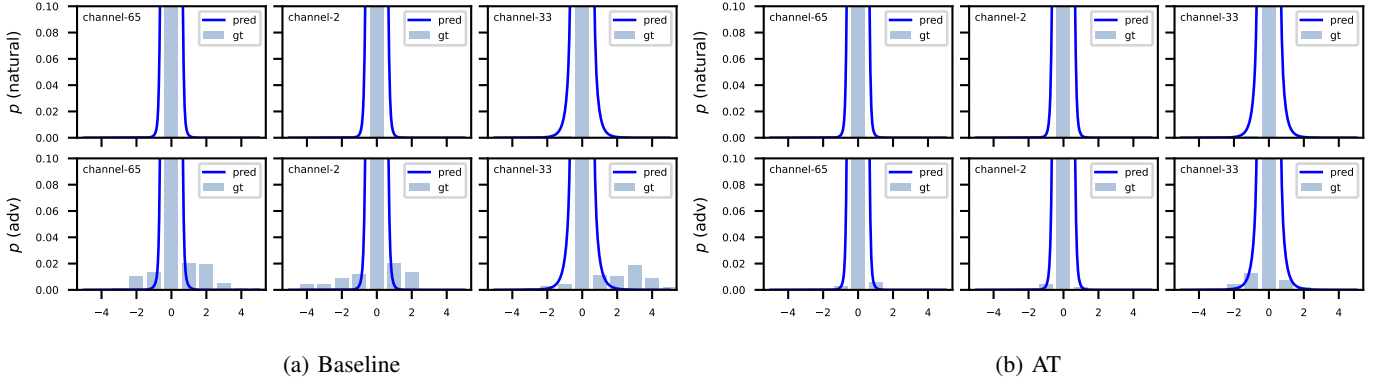


Fig. 10: Illustration of the divergence between predicted distribution (pred) by the entropy estimator and actual distribution (gt) of the latent features to be entropy coded. The model used here is MS-SSIM optimized Ballé2018 with quality level $q=5$. ‘Kodim03’ in Kodak is used as the natural image and for generating the corresponding adversarial example. Three channels with the largest divergence are exemplified for illustration.

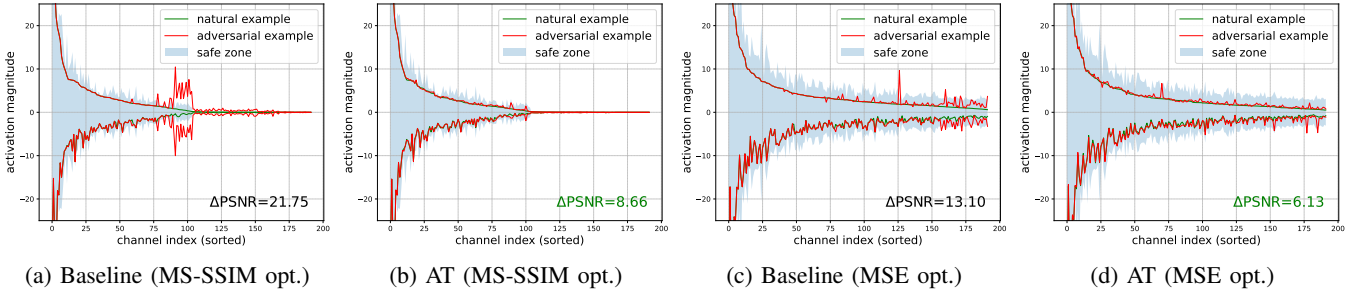


Fig. 11: The magnitude range of channel-wise activation at the bottleneck layer for both the original baseline model and adversarially retrained model. Both MSE and MS-SSIM optimized Ballé2018 models are tested and ‘Kodim09’ is used as an example here as the natural image and also for generating the corresponding adversarial example. The channels are sorted in descending order of the activation magnitude of the natural example.

As also listed in Table III, besides the degradation in reconstruction quality, the compressed bitrate is generally increased for adversarial examples, which reveals that the injected noise is more difficult to model for efficient compression.

$$R = - \sum_{\hat{z}} p(\hat{z}) \log_2 q(\hat{z}) \quad (12)$$

We thus visualized the actual distribution of the latent features $p(\hat{z})$ and the corresponding distribution $q(\hat{z})$ predicted by the entropy estimator in Fig. 10a. The final bitrate R is determined by the cross entropy between $p(\hat{z})$ and $q(\hat{z})$ as in (12). As seen, the actual distribution of the adversarial example diverges significantly from the predicted distribution, yielding inaccurate entropy modeling and bitrate increase.

2) *NIC settings*: Different from existing rules-based JPEG, VVC Intra, etc, the learning-based NIC solutions usually train separate models for different quality metrics and target bitrates.

Loss functions. The MSE and MS-SSIM are two commonly used quality metrics in image compression. They have also been widely applied as loss functions for training NIC models. As in Table III, we test various MSE and MS-SSIM optimized methods and mixed loss function (MSE+LPIPS+GAN) based HiFiC, exhibiting successful attacks regardless of the loss function used in model optimization.

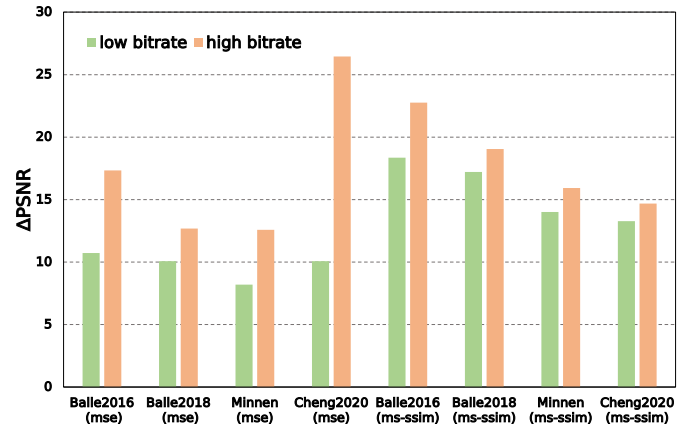


Fig. 12: **Impact of Quality Scales and Loss functions Used in NICs.** The “low bitrate” and “high bitrate” separately represent averaged results of models for low-quality scales ($q = 1,2,3$) and high-quality scales ($q = 4,5,6$). More information about the setting of the quality scale q can be found in Table I.

When comparing MSE and MS-SSIM optimized models from the perspective of latent activations in Fig. 11a and Fig. 11c, we can clearly see that the activations of compressed adversarial example using the MS-SSIM optimized model

vary more significantly than that using the MSE optimized model, which is consistent with the overall measurement of Δ PSNR in Table III that MS-SSIM optimized models are more vulnerable to adversarial attacks in most cases.

Quality Scales. In practice, images will be encoded at various quality scales (or bit rates) to satisfy diverse application requests. Generally, a larger bit rate would come with better reconstruction quality. However, as shown in Fig. 12, the NIC models are constantly vulnerable to adversarial attacks at all quality scales. Actually, due to the irreversibility of VAE-based methods as mentioned in (2), there exists a distortion up-bound or **AE limit** φ in (13) as mentioned in [38] no matter how the bitrate r increases, i.e.,

$$\lim_{r \rightarrow +\infty} \|x - f_D(f_E(x))\| = \varphi. \quad (13)$$

It explains why it is applicable to generate adversarial examples for models trained for arbitrary bitrates.

Along with the increase of compressed bitrate, the quality of adversarial reconstruction gets even worse. We believe that it is because, at low bitrates, even though adversarial examples are with the perturbation, a higher quantization level would remove more details as well as noises, which could partially stop the noise accumulation and present fewer distortions. However, when the bitrate gets higher, the model tries to retain more information of the input image, which may also accumulate the perturbation layer by layer to produce severer distortion.

Attack Transferability. Another area that has received extensive attention is the transferability [63]–[66] of adversarial perturbations. In Fig. 13 we present some preliminary tests of the transferability. For cross-image transferability, specifically, the adversarial perturbations generated for a specific image are directly added to other images to test the transferability of the adversarial perturbation. Noticeable distortions are consistently presented in adversarial reconstructions with Δ PSNR measurement shown in Fig. 13(a), which means it is possible to generate universal perturbations that can widely affect the rate-distortion performance of multiple samples. Besides the transferability of adversarial perturbation across different images, there are many other aspects worth deep investigation, such as the transferability across different networks, which we also present in Fig. 13b-c. The results indicate that the transferability across different models is relatively small. This is mainly because our approach was not specifically designed for cross-model transferability. Nevertheless, we believe that exploring strategies to improve cross-model transferability is an interesting and challenging direction for future research.

V. ATTACK DEFENSE

Extensive experiments in the last section report that existing NIC models are vulnerable to adversarial attacks, despite different network structures and settings. In this section, we will explore possible defense strategies against adversarial attacks.

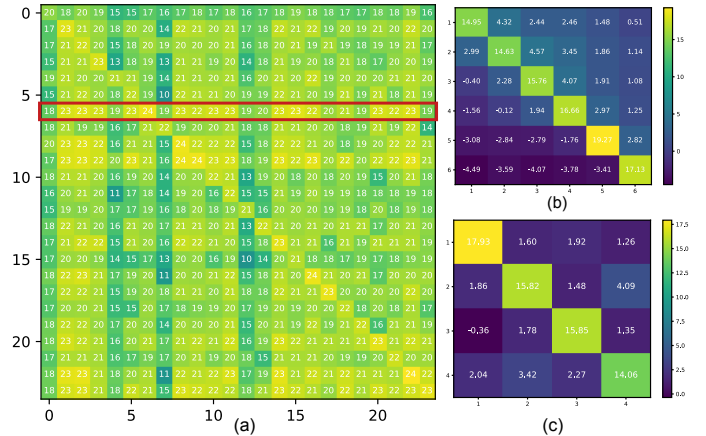


Fig. 13: **Attack transferability measured by Δ PSNR.** (a) **Transferability across images.** Taking “Kodim07.png” as an example (highlighted in a red rectangle), adversarial perturbations generated on Kodim07 (the sixth row) can also cause a similar level of PSNR degradation when being directly augmented on other images. Both indices along with the x - or y -axis indicate the image ID in Kodak. (b) **Transferability across qualities.** Models with the same Ballé2018 network architecture but trained for different quality scales are tested. Indices indicate the quality scales ($q=1-6$). (c) **Transferability across different architectures** (0-Ballé2016, 1-Ballé2018, 2-Minnen, 3-Cheng2020). For (b) and (c), Δ PSNRs over Kodak images are presented.

A. Defense Strategies

Pre-processing. Some pre-processing based defense strategies such as random resizing and JPEG compression would degrade the coding performance even without attack, making them not suitable for image compression tasks (see Fig. 16 and Fig. 17). However, there still exist certain transformations such as flipping and rotations at specific angles (90° , 180° , 270°) that do not have negligible impact on the coding performance without attack. Also, such geometric transformations have been proven to be able to mitigate the effect of adversarial perturbation [27], [67], [68]. Therefore we choose the geometric self-ensemble [52] as one of the defense strategies for evaluation.

Geometric self-ensemble (ensemble for short) was first proposed to improve the performance of super-resolution networks. It generates several augmented adversarial inputs $x_i^* = T_i(x)$ for each input image by flipping and rotation, where T_i represents eight geometric transformations in total. With these augmented inputs, we can generate corresponding reconstruction images $\{\hat{x}_1^*, \dots, \hat{x}_8^*\}$ using the NIC networks. We then apply inverse transform to those output images to get $\hat{x}_i^* = T_i^{-1}(\hat{x}_i^*)$. Finally, we select the transformed output with minimum distortion compared with the original input x as the final self-ensemble result. Besides, an extra transformation index i needs to be stored in the bitstream to help the decoder to apply the correct inverse transform.

Adversarial Training. Note that preprocessing (transformation) based defense strategies only apply process on the

Algorithm 1 Adversarial Training

Input: Encoder $f_E()$ parameters θ , Decoder $f_D()$ parameters ϕ , Dataset \mathbb{D} , finetuning iterations N , adversarial example generation iterations M , RDO penalty λ ;

Output: θ^*, ϕ^*

```

1:  $\theta^*, \phi^* = \theta, \phi$  //initialize using pretrained baseline model
2: for  $i < N$  do
3:    $\vec{x}_{\text{ori}} = \text{RANDOM\_SAMPLE\_FROM}(\mathbb{D})$ 
4:    $\mathbf{n} = \text{RANDOM\_NOISE}()$ ,  $\vec{x}^* = \vec{x}_{\text{ori}} + \mathbf{n}$ 
5:   for  $j \leq M$  do
6:     optimize  $\vec{x}^*$  by Eq. (6)
7:      $j = j + 1$ 
8:   end for
9:    $dloss = \text{DISTORTION\_FUNCTION}(f_D(f_E(\vec{x}^*)), \vec{x}^*)$ 
10:   $rloss = \text{RATE\_FUNCTION}(f_E(\vec{x}^*))$ 
11:   $loss = \lambda dloss + rloss$ 
12:   $\theta^* = \text{OPTIMIZER}(\theta^*, loss)$ 
13:   $\phi^* = \text{OPTIMIZER}(\phi^*, loss)$ 
14:   $i = i + 1$ 
15: end for
16:
17: return  $\theta^*, \phi^*$ 

```

input images while keeping the models unchanged. Besides, multiple transformed input images need to be compressed and reconstructed to find the optimal output, making the computational complexity multiple times greater. Therefore, the robustness improvement of the model itself is also highly worth investigating.

Existing NIC approaches often use noise-free (or at least less noise), high-quality, uncompressed image datasets to train respective models. They work well on clean and uncompressed content but are possibly vulnerable to noisy inputs as aforementioned. Experiments in previous sections have shown that such noisy inputs can be simulated by adversarial example generation, we then propose to utilize these generated adversarial examples for model finetuning, by which we can enrich the distribution of training data and effectively improve the model generalization.

As described in Algorithm 1, we iteratively implement the attack-and-finetune strategy to update the pretrained model. Here θ, ϕ are trainable parameters in encoder $f_E()$ and decoder $f_D()$ respectively. N is the total iterations of adversarial training and in each iteration, a batch of 8 images are randomly sampled from the training dataset \mathbb{D} . These original images \vec{x}_{ori} will be used to generate adversarial examples \vec{x}^* with M steps of optimization following (6), and then \vec{x}^* will be fed into the network to update the pretrained models with Adam optimizer. In this paper, we set $N = 1000$, $M = 300$. Randomly-cropped $256 \times 256 \times 3$ patches from Vimeo90K [69] are used as the training baseline dataset \mathbb{D} . Note that l_2 distance is used and two noise threshold level settings ($\epsilon = 1e^{-3}$ and $1e^{-4}$) are applied and compared. The generation of each batch of adversarial examples costs about 22s on the platform with Intel Xeon Silver 4210 CPU@2.20GHz and a single NVIDIA RTX 2080Ti GPU.

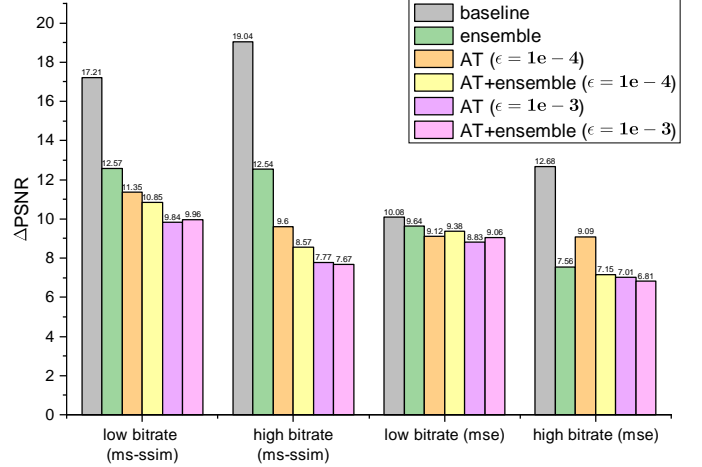


Fig. 14: **Robustness Improvement Comparison.** Baseline models (baseline) are pretrained NIC models, provided by publicly available resources [61]. The ensemble strategy is also directly applied to the pretrained baseline models. Adversarial retrained models (AT) are finetuned from the baseline models with two perturbation levels ($\epsilon=1e^{-4}$ and $\epsilon=1e^{-3}$). The AT+ensemble means applying the self-ensemble strategy to the AT models. The results are averaged across all Kodak images. The “low bitrate” and “high bitrate” separately represent averaged results of models for low-quality scales ($q = 1, 2, 3$) and high-quality scales ($q = 4, 5, 6$) in Table I.

B. Defense Efficiency

We mainly show the efficiency of attack defense in two folds: one aspect is about the robustness improvement both visually and quantitatively; the other one is about the coding efficiency of the NIC models with the defense algorithm integrated. Here, the Ballé2018 method is first used as an example to evaluate the impact of different defense strategies on defense efficiency in Fig. 14-17. More comprehensive results for different models and settings can be found in Table IV.

1) *Robustness Improvement:* In Fig. 14, the defense efficiency measured by ΔPSNR is displayed. The **ensemble** strategy, two input perturbation threshold levels during adversarial training (**AT**), and their combination (**AT+ensemble**) are tested and compared. Note that the AT ($\epsilon = 1e^{-4}$ and $\epsilon = 1e^{-3}$) here only indicates the perturbation levels used in training. While testing the defense efficiency, the input perturbation is consistently set to $1e^{-4}$.

Experiments clearly show that both the self-ensemble strategy and adversarial training can effectively improve the robustness of underlying models and usually AT models can achieve better defense performance compared with the self-ensemble strategy. For AT models, more robustness improvement can be achieved with a larger perturbation level ϵ during adversarial training. Besides, when ϵ during training is set low ($\epsilon = 1e^{-4}$), the combination of AT and self ensemble can further improve defense efficiency, while when ϵ is already high, the additional application of self ensemble can no longer provide

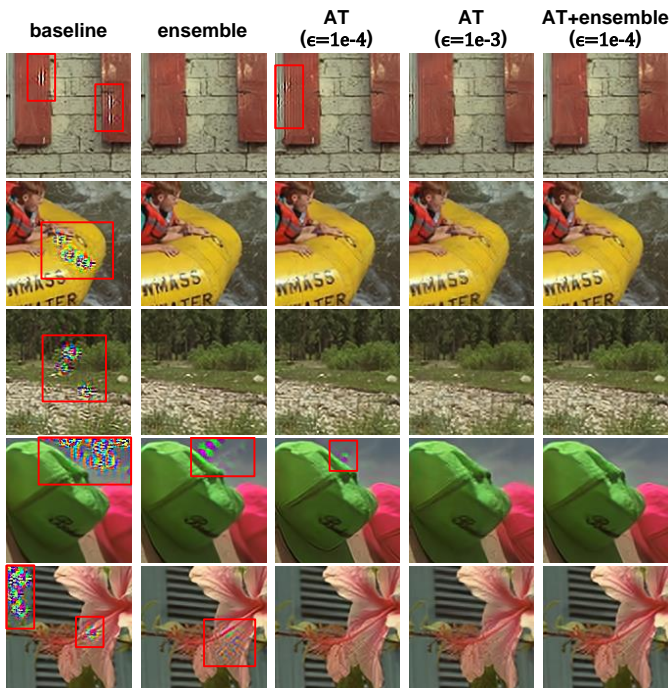


Fig. 15: Visual comparison of the defense efficiency of different strategies. The tested models here are MS-SSIM optimized Ballé2018 with quality scale $q = 5$.

an obvious performance gain. Figure 15 further visualizes the reconstructions of adversarial examples with different defense strategies. It is also well observed that the distortions caused by the adversarial attack are effectively suppressed.

In addition to the above subjective and objective comparisons, Fig. 11 shows the activation magnitude comparison between natural images and adversarial examples for both the baseline model and adversarially retrained model. For model trained on natural images in Fig. 11a and 11c, the activation of adversarial examples shows distinct changes compared with natural images. While for AT models retrained on adversarial examples, the activation inconsistency in Fig. 11b and 11d is greatly alleviated. Previous work on the defense of image classification networks [70] has also presented similar phenomena. Besides, compared with the distribution of the baseline model shown in Fig. 10a, Here in Fig. 10b for the adversarially trained model, the divergence between the predicted distribution and actual distribution is greatly alleviated. As a result, the bitrate gain caused by adversarial perturbation can also be better controlled now. More experimental results on different methods can be found in Table IV.

Another two preprocessing-based defense strategies (spatial resizing and bit depth reduction) are also included for comparison. For the methods using bit-depth reduction, the original input image with a bit depth equal to 8 is truncated to lower bit depths, e.g., 2, 4, 6, to reduce the impact of adversarial perturbations. Similarly, spatial resizing downsamples the original image to a smaller size at a factor of 0.5, 0.75, or 0.85 and correspondingly upsamples them to the original resolution for future applications. As shown in Fig. 16, these methods can alleviate the PSNR degradation incurred

TABLE IV: The Δbpp and ΔPSNR of adversarial examples compared with original images for different defense strategies. For a fair comparison, the AT models here are AT($\epsilon=1e-4$) since this setting would not degrade the original coding efficiency. Results are averaged over all 6 quality levels and both mse and ms-ssim optimized models on the Kodak dataset. Lower Δbpp and ΔPSNR mean better defense efficiency.

Methods	Defense Strategy	$\Delta\text{bpp}\downarrow$	$\Delta\text{PSNR}\downarrow$
Ballé2016	baseline (no defense)	4.74%	17.29
	ensemble	3.66%	12.73
	AT	2.23%	11.54
	AT+ensemble	3.15%	8.98
Ballé2018	baseline (no defense)	8.37%	13.80
	ensemble	7.62%	8.60
	AT	6.51%	9.79
	AT+ensemble	5.63%	8.27
Minnen	baseline (no defense)	10.46%	12.68
	ensemble	9.27%	10.86
	AT	9.89%	8.90
	AT+ensemble	9.32%	8.62
Cheng2020	baseline (no defense)	62.90%	16.13
	ensemble	9.26%	10.82
	AT	12.60%	10.60
	AT+ensemble	9.01%	9.14

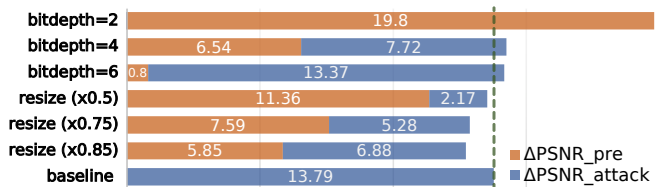


Fig. 16: **Defense efficiency using different pre-processing strategies.** ΔPSNR_{pre} indicates the PSNR degradation directly caused by the pre-processing strategies like resizing or bit depth reduction. $\Delta\text{PSNR}_{attack}$ is the further quality degradation caused by adversarial attack after applying the defense. The overall quality degradation equals the sum of ΔPSNR_{pre} and $\Delta\text{PSNR}_{attack}$. Here pretrained Ballé2018 models are tested and used as the baseline.

by the adversarial perturbation. However, both spatial resizing and bit depth reduction in pre-processing inevitably introduce additional quality degradation, leading to similar or even worse overall degradation when compared with the anchor using baseline models without applying any defense strategies at all.

2) *Coding Efficiency*: Previous discussions show that NIC models can effectively defend against attacks through defense strategies. Another important question then arises: whether the coding efficiency for original natural images is retained after applying defense strategies. Figure 17 shows the rate-distortion curves averaged over Kodak images. As aforementioned, pre-processing strategies like spatial resizing and bit depth reduction significantly degraded the performance even for clean natural images, while self-ensemble based defense strategy will not degrade the original coding performance for both baseline models as well as AT models.

For the adversarially trained models with two perturbation levels during training, when the perturbation level is lower ($\epsilon=1e-4$), the coding efficiency of AT models roughly aligns with the pretrained baseline models. However, as the input

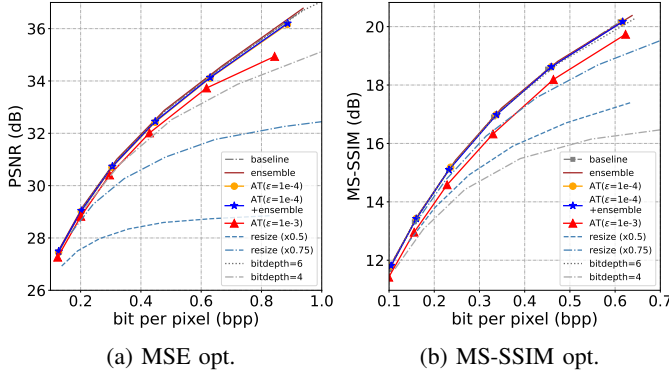


Fig. 17: **Coding Efficiency.** Rate-distortion efficiency averaged over Kodak images. Ballé2018 [2] models are exemplified.

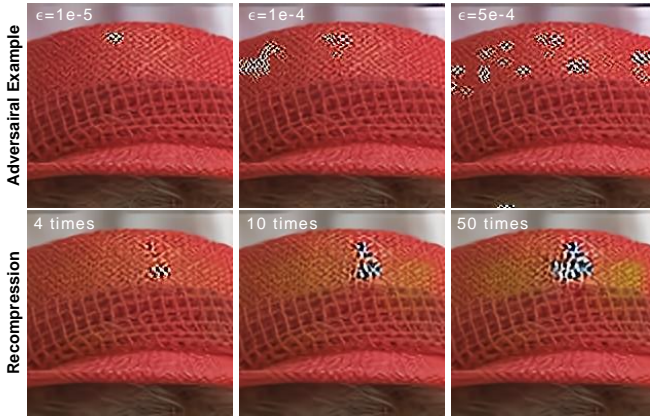


Fig. 18: **Visualization of similar distortion pattern caused by image recompression and adversarial perturbation.** A pretrained Ballé2018 baseline model is tested as an example. The first row is the reconstructions of adversarial examples generated under different perturbation levels ϵ . The second row is reconstructions after different times of recompression.

perturbation increases to $\epsilon=1e-3$, although the robustness can be further improved as in Fig. 15, the coding efficiency of AT models starts to deteriorate significantly, especially at high bitrates. Therefore, by setting appropriate input perturbation thresholds during training, the adversarial training could not only effectively improve the model robustness, but also clearly retain the coding efficiency of the original model.

In summary, these defense strategies can be easily integrated into existing learned compression codecs without requiring any changes to the underlying compression framework. Extensive experiments show that the proposed defense solutions are simple, effective, and generalizable to most existing neural image compression approaches.

C. Recompression Application

Looking back to the instability problem of learned image recompression mentioned at the beginning of the paper, to tackle it, Kim *et. al* [18] proposed to include images that were repeatedly compressed in training to improve the model robustness on purpose. Here, we want to evaluate whether

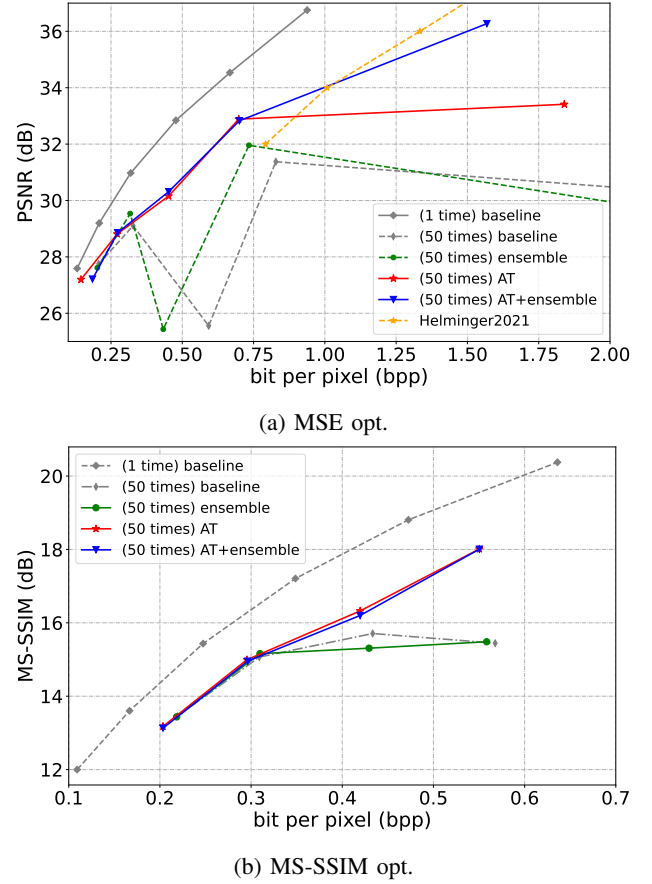


Fig. 19: **Coding efficiency degradation comparison averaged over Kodak images.** Ballé2018 models are tested and the AT models are trained with $\epsilon=1e-4$.

our proposed defense strategies that are not designed for any specific scenario can also improve the model robustness more generally.

Examples in Fig. 18 show that some of the distortions caused by recompression are of high similarity to examples generated by adversarial attacks. Such similar patterns prove that the adversarially trained models can also be generalized to practical applications like image recompression. The visual comparison using Kodak images is shown in Fig. 1. After 50 repetitions of recompression, severe distortions can be found in reconstructions encoded using the pretrained baseline model, while these unexpected distortions are greatly alleviated in decoded images that were compressed using the AT model.

Figure 19 further shows the overall rate-distortion comparison for recompression at different bit rates. As seen, the performance of the baseline model degrades significantly after 50 times recompression. We can also clearly see from the rate-distortion curves that models with higher quality scales are with severer quality degradation, which is consistent with our observation in Sec. IV-D by the adversarial attack. This also evidences that our proposed adversarial attack-based robustness evaluation method can really be indicative of the robustness of the NIC models in practical applications.

For different defense strategies, the self-ensemble strat-

egy provides limited performance improvement, while the adversarial training strategy still works well by significantly decreasing the quality degradation caused by image recompression. This clearly shows the generalization of our proposed adversarial training strategy. We also expect that our methodology can be applied to other pixel domain regression tasks for robustness evaluation and improvement in future works such as quality enhancement, super-resolution, etc.

VI. CONCLUSION

In this paper, we propose to generate adversarial examples to examine the model robustness of existing learned image compression methods. Experiments show that all tested methods are vulnerable to adversarial attacks regardless of their network architectures, loss functions, and quality settings. To tackle it, we then explore defense strategies to improve the robustness of NIC models. Results have shown the effectiveness of our methodology, not only successfully defending the adversarial attack with great distortion alleviation in reconstruction, but also retaining the outstanding compression performance. It is also demonstrated that our methodology can be easily extended to the targeted attack. Our proposed method is generalizable to the most popular learned image compression frameworks and can be applied to other pixel domain regression tasks as well in future works.

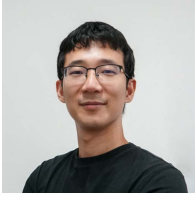
VII. ACKNOWLEDGEMENT

We are very grateful for the authors of [1], [2], [4]–[7], [39] who have made their learning-based image compression methods open source to the public.

REFERENCES

- [1] J. Ballé, V. Laparra, and E. P. Simoncelli, “End-to-end optimized image compression,” *arXiv preprint arXiv:1611.01704*, 2016. 1, 3, 4, 8, 14
- [2] J. Ballé, D. Minnen, S. Singh, S. J. Hwang, and N. Johnston, “Variational image compression with a scale hyperprior,” *arXiv preprint arXiv:1802.01436*, 2018. 1, 3, 4, 8, 13, 14
- [3] M. Li, W. Zuo, S. Gu, D. Zhao, and D. Zhang, “Learning convolutional networks for content-weighted image compression,” in *Proceedings of the IEEE Conference on Computer Vision and Pattern Recognition*, 2018, pp. 3214–3223. 1
- [4] D. Minnen, J. Ballé, and G. D. Toderici, “Joint autoregressive and hierarchical priors for learned image compression,” in *Advances in Neural Information Processing Systems*, 2018, pp. 10 794–10 803. 1, 3, 4, 8, 14
- [5] F. Mentzer, G. Toderici, M. Tschannen, and E. Agustsson, “High-fidelity generative image compression,” *arXiv preprint arXiv:2006.09965*, 2020. 1, 4, 8, 14
- [6] Z. Cheng, H. Sun, M. Takeuchi, and J. Katto, “Learned image compression with discretized gaussian mixture likelihoods and attention modules,” in *2020 IEEE/CVF Conference on Computer Vision and Pattern Recognition, CVPR 2020, Seattle, WA, USA, June 13-19, 2020*. IEEE, 2020, pp. 7936–7945. [Online]. Available: <https://doi.org/10.1109/CVPR42600.2020.00796> 1, 3, 4, 8, 14
- [7] T. Chen, H. Liu, Z. Ma, Q. Shen, X. Cao, and Y. Wang, “End-to-end learnt image compression via non-local attention optimization and improved context modeling,” *IEEE Transactions on Image Processing*, vol. 30, pp. 3179–3191, 2021. 1, 3, 4, 8, 14
- [8] Y. Hu, W. Yang, Z. Ma, and J. Liu, “Learning end-to-end lossy image compression: A benchmark,” *IEEE Transactions on Pattern Analysis and Machine Intelligence*, 2021. 1
- [9] M. Lu, P. Guo, H. Shi, C. Cao, and Z. Ma, “Transformer-based image compression,” in *2022 Data Compression Conference (DCC)*, 2022, pp. 469–469. 1
- [10] S. Ma, X. Zhang, C. Jia, Z. Zhao, S. Wang, and S. Wang, “Image and video compression with neural networks: A review,” *IEEE Transactions on Circuits and Systems for Video Technology*, vol. 30, no. 6, pp. 1683–1698, 2020. 1
- [11] G. K. Wallace, “The jpeg still picture compression standard,” *Communications of the ACM*, vol. 34, no. 4, pp. 30–44, 1991. 1, 3
- [12] D. T. Lee, “Jpeg 2000: Retrospective and new developments,” *Proceedings of the IEEE*, vol. 93, no. 1, pp. 32–41, Jan 2005. 1, 3
- [13] B. Bross, Y.-K. Wang, Y. Ye, S. Liu, J. Chen, G. J. Sullivan, and J.-R. Ohm, “Overview of the versatile video coding (vvc) standard and its applications,” *IEEE Transactions on Circuits and Systems for Video Technology*, vol. 31, no. 10, pp. 3736–3764, 2021. 1, 3
- [14] Z. Li, H. Liu, L. Yang, and Z. Ma, “In-camera raw compression: A new paradigm from image acquisition to display,” in *54th Asilomar Conference on Signals, Systems, and Computers, ACSSC 2020, Pacific Grove, CA, USA, November 1-4, 2020*, M. B. Matthews, Ed. IEEE, 2020, pp. 1132–1136. [Online]. Available: <https://doi.org/10.1109/IEEECONF51394.2020.9443315> 1
- [15] Z. Wang, E. P. Simoncelli, and A. C. Bovik, “Multiscale structural similarity for image quality assessment,” in *Signals, Systems and Computers, 2004. Conference Record of the Thirty-Seventh Asilomar Conference on*, vol. 2. Ieee, 2003, pp. 1398–1402. 1, 5
- [16] X. Wang, T. Chen, and Z. Ma, “Subjective quality optimized efficient image compression,” in *Proceedings of the IEEE/CVF Conference on Computer Vision and Pattern Recognition*, 2021, pp. 1911–1915. 1
- [17] J. Xu, R. Joshi, and R. A. Cohen, “Overview of the emerging hevce screen content coding extension,” *IEEE Transactions on Circuits and Systems for Video Technology*, vol. 26, no. 1, pp. 50–62, 2016. 1
- [18] J.-H. Kim, S. Jang, J.-H. Choi, and J.-S. Lee, “Instability of successive deep image compression,” ser. MM ’20. New York, NY, USA: Association for Computing Machinery, 2020, p. 247–255. [Online]. Available: <https://doi.org/10.1145/3394171.3413680> 2, 13
- [19] J. Choi and B. Han, “Task-aware quantization network for jpeg image compression,” in *European Conference on Computer Vision*. Springer, 2020, pp. 309–324. 2
- [20] I. J. Goodfellow, J. Shlens, and C. Szegedy, “Explaining and harnessing adversarial examples,” in *3rd International Conference on Learning Representations, ICLR 2015, San Diego, CA, USA, May 7-9, 2015, Conference Track Proceedings*, 2015. 2, 3, 4
- [21] I. Goodfellow, J. Shlens, and C. Szegedy, “Explaining and harnessing adversarial examples,” in *International Conference on Learning Representations*, 2015. [Online]. Available: <http://arxiv.org/abs/1412.6572> 2, 4
- [22] A. Nguyen, J. Yosinski, and J. Clune, “Deep neural networks are easily fooled: High confidence predictions for unrecognizable images,” in *Proceedings of the IEEE conference on computer vision and pattern recognition*, 2015, pp. 427–436. 2
- [23] C. Xiao, R. Deng, B. Li, F. Yu, M. Liu, and D. Song, “Characterizing adversarial examples based on spatial consistency information for semantic segmentation,” in *Proceedings of the European Conference on Computer Vision (ECCV)*, September 2018. 2
- [24] X. Wei, S. Liang, N. Chen, and X. Cao, “Transferable adversarial attacks for image and video object detection,” in *Proceedings of the Twenty-Eighth International Joint Conference on Artificial Intelligence, IJCAI-19*. International Joint Conferences on Artificial Intelligence Organization, 7 2019, pp. 954–960. [Online]. Available: <https://doi.org/10.24963/ijcai.2019/134> 2
- [25] M. Yin, Y. Zhang, X. Li, and S. Wang, “When deep fool meets deep prior: Adversarial attack on super-resolution network,” in *Proceedings of the 26th ACM International Conference on Multimedia*, ser. MM ’18. New York, NY, USA: Association for Computing Machinery, 2018, p. 1930–1938. [Online]. Available: <https://doi.org/10.1145/3240508.3240603> 2, 4
- [26] A. Ranjan, J. Janai, A. Geiger, and M. J. Black, “Attacking optical flow,” in *Proceedings of the IEEE International Conference on Computer Vision*, 2019, pp. 2404–2413. 2, 4
- [27] J.-H. Choi, H. Zhang, J.-H. Kim, C.-J. Hsieh, and J.-S. Lee, “Deep Image Destruction: A Comprehensive Study on Vulnerability of Deep Image-to-Image Models against Adversarial Attacks,” *arXiv:2104.15022 [cs, eess]*, Apr. 2021, arXiv: 2104.15022. [Online]. Available: <http://arxiv.org/abs/2104.15022> 2, 4, 6, 10
- [28] N. Carlini and D. Wagner, “Towards Evaluating the Robustness of Neural Networks,” *arXiv:1608.04644 [cs]*, Mar. 2017, arXiv: 1608.04644. [Online]. Available: <http://arxiv.org/abs/1608.04644> 2, 4, 5
- [29] A. Kurakin, I. Goodfellow, and S. Bengio, “Adversarial examples in the physical world,” *arXiv, Tech. Rep.* arXiv:1607.02533, Feb.

- 2017, arXiv:1607.02533 [cs, stat] type: article. [Online]. Available: <http://arxiv.org/abs/1607.02533> 2, 4, 5
- [30] K. He, X. Zhang, S. Ren, and J. Sun, "Deep residual learning for image recognition," in *Proceedings of the IEEE conference on computer vision and pattern recognition*, 2016, pp. 770–778. 4
- [31] J. Ballé, V. Laparra, and E. P. Simoncelli, "Density modeling of images using a generalized normalization transformation," *arXiv preprint arXiv:1511.06281*, 2015. 4
- [32] V. Nair and G. E. Hinton, "Rectified linear units improve restricted boltzmann machines," in *ICML*, 2010. 4
- [33] N. Ahmed, T. Natarajan, and K. R. Rao, "Discrete cosine transform," *IEEE transactions on Computers*, vol. 100, no. 1, pp. 90–93, 1974. 3
- [34] B.-F. Wu and C.-F. Lin, "A high-performance and memory-efficient pipeline architecture for the 5/3 and 9/7 discrete wavelet transform of jpeg2000 codec," *IEEE Transactions on Circuits and Systems for Video Technology*, vol. 15, no. 12, pp. 1615–1628, 2005. 3
- [35] J. Zepeda, C. Guillemot, and E. Kijak, "Image compression using sparse representations and the iteration-tuned and aligned dictionary," *IEEE Journal of Selected Topics in Signal Processing*, vol. 5, no. 5, pp. 1061–1073, 2011. 3
- [36] Y. Xue and Y. Wang, "Video coding using a self-adaptive redundant dictionary consisting of spatial and temporal prediction candidates," in *2014 IEEE International Conference on Multimedia and Expo (ICME)*, 2014, pp. 1–6. 3
- [37] J. Lee, S. Cho, and S.-K. Beack, "Context-adaptive entropy model for end-to-end optimized image compression," *arXiv preprint arXiv:1809.10452*, 2018. 3
- [38] L. Helming, A. Djelouah, M. Gross, and C. Schroers, "Lossy image compression with normalizing flows," in *Neural Compression: From Information Theory to Applications – Workshop @ ICLR 2021*, 2021. [Online]. Available: <https://openreview.net/forum?id=NQJ9pMf9id> 3, 10
- [39] Y. Xie, K. L. Cheng, and Q. Chen, "Enhanced invertible encoding for learned image compression," in *Proceedings of the ACM International Conference on Multimedia*, 2021. 3, 4, 8, 14
- [40] S.-M. Moosavi-Dezfooli, A. Fawzi, and P. Frossard, "Deepfool: A simple and accurate method to fool deep neural networks," in *Proceedings of the IEEE Conference on Computer Vision and Pattern Recognition (CVPR)*, June 2016. 3, 4
- [41] R. Zhang, P. Isola, A. A. Efros, E. Shechtman, and O. Wang, "The unreasonable effectiveness of deep features as a perceptual metric," in *Proceedings of the IEEE conference on computer vision and pattern recognition*, 2018, pp. 586–595. 4
- [42] W. Hong, T. Chen, M. Lu, S. Pu, and Z. Ma, "Efficient neural image decoding via fixed-point inference," *IEEE Transactions on Circuits and Systems for Video Technology*, vol. 31, no. 9, pp. 3618–3630, 2021. 4, 8
- [43] C. Szegedy, W. Zaremba, I. Sutskever, J. Bruna, D. Erhan, I. Goodfellow, and R. Fergus, "Intriguing properties of neural networks," *arXiv preprint arXiv:1312.6199*, 2013. 4
- [44] A. Madry, A. Makelov, L. Schmidt, D. Tsipras, and A. Vladu, "Towards Deep Learning Models Resistant to Adversarial Attacks," Sep. 2019, arXiv:1706.06083 [cs, stat]. [Online]. Available: <http://arxiv.org/abs/1706.06083> 4
- [45] A. Ganeshan, V. B. S., and V. B. Radhakrishnan, "Fda: Feature disruptive attack," in *2019 IEEE/CVF International Conference on Computer Vision (ICCV)*, 2019, pp. 8068–8078. 4
- [46] A. Madry, A. Makelov, L. Schmidt, D. Tsipras, and A. Vladu, "Towards deep learning models resistant to adversarial attacks," *arXiv preprint arXiv:1706.06083*, 2017. 4
- [47] Y. Dong, F. Liao, T. Pang, H. Su, J. Zhu, X. Hu, and J. Li, "Boosting Adversarial Attacks with Momentum," in *2018 IEEE/CVF Conference on Computer Vision and Pattern Recognition*. Salt Lake City, UT: IEEE, Jun. 2018, pp. 9185–9193. [Online]. Available: <https://ieeexplore.ieee.org/document/8579055/> 4
- [48] D. P. Kingma and J. Ba, "Adam: A method for stochastic optimization," *arXiv:1412.6980v9*, Jan. 2017. 4, 8
- [49] G. K. Dziugaite, Z. Ghahramani, and D. M. Roy, "A study of the effect of jpg compression on adversarial images," *arXiv preprint arXiv:1608.00853*, 2016. 4
- [50] C. Xie, J. Wang, Z. Zhang, Z. Ren, and A. Yuille, "Mitigating Adversarial Effects Through Randomization," *arXiv, Tech. Rep. arXiv:1711.01991*, Feb. 2018, arXiv:1711.01991 [cs] type: article. [Online]. Available: <http://arxiv.org/abs/1711.01991> 4
- [51] W. Xu, D. Evans, and Y. Qi, "Feature Squeezing: Detecting Adversarial Examples in Deep Neural Networks," *Tech. Rep.*, Dec. 2017, arXiv:1704.01155 [cs]. [Online]. Available: <http://arxiv.org/abs/1704.01155> 4
- [52] B. Lim, S. Son, H. Kim, S. Nah, and K. M. Lee, "Enhanced Deep Residual Networks for Single Image Super-Resolution," *arXiv:1707.02921 [cs]*, Jul. 2017, arXiv: 1707.02921. [Online]. Available: <http://arxiv.org/abs/1707.02921> 4, 10
- [53] C. Szegedy, W. Zaremba, I. Sutskever, J. Bruna, D. Erhan, I. Goodfellow, and R. Fergus, "Intriguing properties of neural networks," in *International Conference on Learning Representations*, 2014. [Online]. Available: <http://arxiv.org/abs/1312.6199> 4
- [54] R. Huang, B. Xu, D. Schuurmans, and C. Szepesvari, "Learning with a strong adversary," *Computer Science*, 2015. 4
- [55] A. Kurakin, D. Boneh, F. Tramèr, I. Goodfellow, N. Papernot, and P. McDaniel, "Ensemble adversarial training: Attacks and defenses," 2018. [Online]. Available: <https://openreview.net/pdf?id=rkZvSe-RZ> 4
- [56] P. Tabacof, J. Tavares, and E. Valle, "Adversarial images for variational autoencoders," *ArXiv*, vol. abs/1612.00155, 2016. 4
- [57] J. Kos, I. Fischer, and D. Song, "Adversarial examples for generative models," in *2018 IEEE security and privacy workshops (spw)*. IEEE, 2018, pp. 36–42. 4, 5
- [58] A. B. L. Larsen, S. K. Sønderby, H. Larochelle, and O. Winther, "Autoencoding beyond pixels using a learned similarity metric," in *ICML'16 Proceedings of the 33rd International Conference on International Conference on Machine Learning - Volume 48*, 2016, pp. 1558–1566. 4
- [59] Y. Netzer, T. Wang, A. Coates, A. Bissacco, B. Wu, and A. Y. Ng, "Reading digits in natural images with unsupervised feature learning," 2011. 4
- [60] J.-H. Choi, H. Zhang, J.-H. Kim, C.-J. Hsieh, and J.-S. Lee, "Evaluating robustness of deep image super-resolution against adversarial attacks," in *Proceedings of the IEEE/CVF International Conference on Computer Vision*, 2019, pp. 303–311. 4
- [61] J. Bégin, F. Racapé, S. Feltman, and A. Pushparaja, "Compressai: a pytorch library and evaluation platform for end-to-end compression research," *arXiv preprint arXiv:2011.03029*, 2020. 8, 11
- [62] E. Kodak. Kodak lossless true color image suite (photoncd pcd0992). [Online]. Available: <http://r0k.us/graphics/kodak/> 8
- [63] C. Li, S. Gao, C. Deng, D. Xie, and W. Liu, "Cross-modal learning with adversarial samples," *Advances in neural information processing systems*, vol. 32, 2019. 10
- [64] M. Li, C. Deng, T. Li, J. Yan, X. Gao, and H. Huang, "Towards transferable targeted attack," in *Proceedings of the IEEE/CVF Conference on Computer Vision and Pattern Recognition*, 2020, pp. 641–649. 10
- [65] M. Li, Y. Yang, K. Wei, X. Yang, and H. Huang, "Learning universal adversarial perturbation by adversarial example," in *Proceedings of the AAAI Conference on Artificial Intelligence*, vol. 36, no. 2, 2022, pp. 1350–1358. 10
- [66] X. Yang, C. Deng, K. Wei, J. Yan, and W. Liu, "Adversarial learning for robust deep clustering," *Advances in Neural Information Processing Systems*, vol. 33, pp. 9098–9108, 2020. 10
- [67] D. D. Thang and T. Matsui, "Image Transformation can make Neural Networks more robust against Adversarial Examples," *arXiv, Tech. Rep. arXiv:1901.03037*, Jan. 2019, arXiv:1901.03037 [cs] type: article. [Online]. Available: <http://arxiv.org/abs/1901.03037> 10
- [68] S. Tian, G. Yang, and Y. Cai, "Detecting adversarial examples through image transformation," in *Thirty-second AAAI conference on artificial intelligence*, 2018. 10
- [69] T. Xue, B. Chen, J. Wu, D. Wei, and W. T. Freeman, "Video enhancement with task-oriented flow," *International Journal of Computer Vision (IJCV)*, vol. 127, no. 8, pp. 1106–1125, 2019. 11
- [70] Y. Bai, Y. Zeng, Y. Jiang, S.-T. Xia, X. Ma, and Y. Wang, "Improving Adversarial Robustness via Channel-wise Activation Suppressing," *arXiv:2103.08307 [cs]*, Jan. 2022, arXiv: 2103.08307. [Online]. Available: <http://arxiv.org/abs/2103.08307> 12



Tong Chen received his B.E and M.E. degree in Electronic Science and Engineering from Nanjing University, Jiangsu, China in 2015 and 2018. He is now pursuing the Ph.D. degree in Nanjing University. His current research focuses on image/video processing, including deep learning based image coding. He is a co-recipient of the 2018 PCM Best Paper Finalist, 2020 IEEE MMSP Image Compression Grand Challenge Best Performing Solution.



Zhan Ma is a Professor in the School of Electronic Science and Engineering, Nanjing University, Jiangsu, 210093, China. He received his Ph.D. degree from New York University, New York, in 2011, and his B.S. and M.S. from the Huazhong University of Science and Technology, Wuhan, China, in 2004 and 2006 respectively. From 2011 to 2014, he has been with Samsung Research America, Dallas, TX, and Futurewei Technologies, Inc., Santa Clara, CA, respectively. His research focuses include learned image/video coding and computational imaging. He

was awarded the 2018 PCM Best Paper Finalist, the 2019 IEEE Broadcast Technology Society Best Paper Award, the 2020 IEEE MMSP Grand Challenge Best Image Coding Solution, and the 2023 IEEE WACV Best Algorithms Paper Award.

APPENDIX

A. Distance Measurement

We originally apply the common l_2 distance in (6) for the generation of adversarial examples. Here, we show that other distance metrics like l_1 distance and MS-SSIM measurement can also be used to produce adversarial examples that can also effectively attack NIC models for impaired reconstructions as shown in Fig. 20.

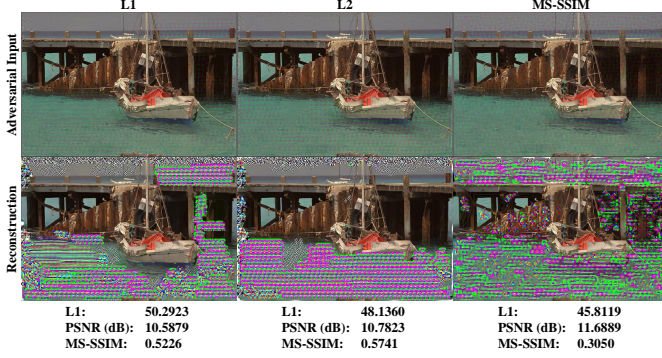


Fig. 20: Illustration of adversarial examples and corresponding adversarial reconstructed images using different distance measurements in (6).

In Table V, we provide more quantitative results. As seen, regardless of the metric used for model training, a higher Δ MS-SSIM loss is observed when MS-SSIM is used as the $\mathcal{D}()$ in (6); while a larger Δ PSNR is presented when $\mathcal{D}()$ uses the L2 (MSE) loss function, regardless of the loss metrics used to train the NIC models. As illustrated in Fig. 21, although the Δ MS-SSIM of Fig. 21(b) is much higher than that of Fig. 21(a), the reconstruction quality of the L2 attacked example is degraded with more visually perceivable impairments. Therefore, Δ PSNR can better reflect the quality degradation incurred by the attack.

TABLE V: Quality evaluation comparison measured by Δ PSNR and Δ MS-SSIM. Kodak datasets and Ballé2018 models are tested.

metrics in \mathcal{D} (attack)	metrics (train)	Δ PSNR	Δ MS-SSIM
MS-SSIM	ms-ssim	8.22	14.11
	mse	5.00	16.05
L2 (MSE)	ms-ssim	16.45	5.65
	mse	11.38	9.20

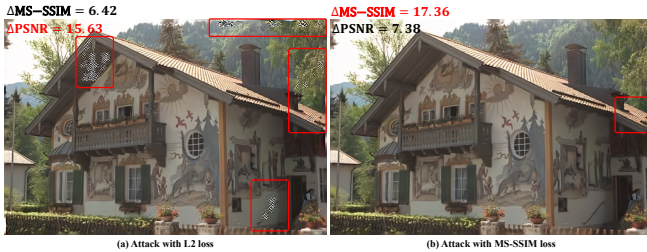


Fig. 21: Visual comparison of distortion using different distance measurements in (6). An MS-SSIM optimized Ballé2018 model is tested.

B. Performance on other types of degradations

We also test the rate-distortion performance of the baseline end-to-end codecs and our proposed defense method (Adversarial Training) on the noisy and blurry degradation in Fig. 22. The results show that the AT models and baseline models show similar performance facing these scenarios. Gaussian random noise and gaussian blur are added to generate degraded input images.

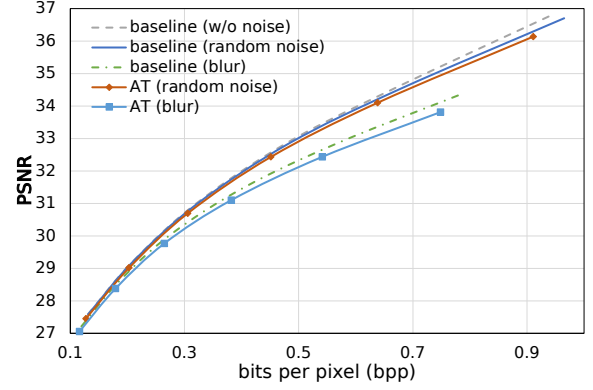


Fig. 22: Rate-Distortion Comparison. Pretrained Ballé2018 models and corresponding AT models are tested. As shown in Fig. 6, the random noise can be suppressed by the compression networks, making the rate-distortion performance on random noise images better than that on blurry images.

C. Detailed Explanations about Δ PSNR

A Linear Example. In order to better clarify our reason for choosing Δ PSNR, we first perform a test on a toy model, which is composed of a single-layer convolution for both the encoder W_1 and decoder W_2 (without non-linear activation function to ensure linearity). In this case, the network is purely linear. Therefore theoretically the amplification level for generated perturbation \mathbf{n}_i added onto input \mathbf{x} can be considered consistent with all different perturbation levels:

$$\begin{aligned}
 \text{with } \hat{\mathbf{x}} &= W_1 W_2 \mathbf{x}, \\
 \hat{\mathbf{x}} + \mathbf{N}_{out} &= W_1 W_2 (\mathbf{x} + \mathbf{n}_i) \\
 &= W_1 W_2 \mathbf{x} + W_1 W_2 \mathbf{n}_i
 \end{aligned} \tag{14}$$

$$\text{now we have: } \mathbf{N}_{out} = W_1 W_2 \mathbf{n}_i$$

$$\text{and: } k\mathbf{N}_{out} = W_1 W_2 (k\mathbf{n}_i)$$

As shown in Fig. 4a, the Δ PSNR keeps the same for all levels over 100dB difference, while even for this linear system the VI still varies with the absolute perturbation level (the larger the absolute input perturbation, the larger the VI would be).

Non-linear System. A more complicated neural network can be very non-linear. Figure 4b shows the vulnerability of a non-linear deep neural network-based image compression network. Δ PSNR now also varies at different perturbation levels for this non-linear network. The results indicate that the network would greatly amplify the attack perturbation of large values.

Note that here the VI values at large input perturbation levels ($< 40\text{dB}$ as exemplified, lower in dB means larger perturbation) become abnormal (< 0) since the output PSNR is now negative. The output distortion is extremely large and has been out of the range of $[0, 1]$.

In practice, we would perform a value clipping operation to the output reconstruction to ensure it is within the range of $[0, 1]$. With clipping operation performed, the results are shown in Fig. 4c. Similar to the observations in Fig. 4a, the VI value still gradually increases as the perturbation level increases. Besides, when the perturbation level reaches a certain threshold, both ΔPSNR and VI metrics exhibit a decline. This doesn't mean that the network is less vulnerable to large perturbations. In fact, this is caused by the value clipping operation. When the input perturbation becomes significantly large, the output distortion can no longer increase due to the clipping operation.

In conclusion, our goal is to eliminate the impact of perturbation magnitude itself on the metrics. This allows us to focus on the model's inherent vulnerability (which can be different at different perturbation levels) but would not being directly biased by the absolute perturbation level.

D. Extending the Methodology to Targeted Attack

This companion section showcases that our methodology can be also applied to targeted attack. Different from the untargeted attack in previous sections that tends to just maximize the reconstruction distortion, A targeted attack is typically applied for semantic content understanding, which attempts to produce a targeted output that is designated to be different from the original output.

1) *Targeted Adversarial Examples*: Assuming that we have the source image \mathbf{x} and a target image \mathbf{x}^t that is different from \mathbf{x} , we hope to generate adversarial input $\mathbf{x}^* = \mathbf{x} + \mathbf{n}$, so that the reconstructed $\hat{\mathbf{x}}^* = f_D(f_E(\mathbf{x}^*))$ would be close to the reconstruction of the target image $\hat{\mathbf{x}}^t = f_D(f_E(\mathbf{x}^t))$. By fixing the encoder $f_E()$ and decoder $f_D()$ of a specific NIC method, the generation of adversarial examples for targeted attack can be formulated as minimizing the input noise as well as the output distance with the target output:

$$\arg \min_{\mathbf{n}} L_t = \begin{cases} \frac{\|\mathbf{n}\|_2^2}{N}, & \frac{\|\mathbf{n}\|_2^2}{N} \geq \epsilon \\ \frac{\|\hat{\mathbf{x}}^* - \hat{\mathbf{x}}^t\|_2^2}{N}, & \frac{\|\mathbf{n}\|_2^2}{N} < \epsilon \end{cases} \quad (15)$$

Similar to (6), here ϵ is the threshold of the input noise to control the perturbation level. The main difference between targeted attack in (15) and untargeted attack in (6) is that: instead of using negative l_2 distance that maximizes the output distortion as in (6), here the objective is to minimize the distance between the reconstruction of target image $\hat{\mathbf{x}}^t$ and the reconstruction of the adversarial example $\hat{\mathbf{x}}^*$.

Note that (15) simply hopes to minimize the distance between the source image and the target image of all pixels, which works well for low-resolution, thumbnail images, such as the handwritten digits dataset MNIST. Nowadays, an image often exhibits a much higher spatial resolution, such as the 4K, 8K, etc, and usually presents multiple semantic cues, e.g., diverse foreground objects, within the same scene, making it

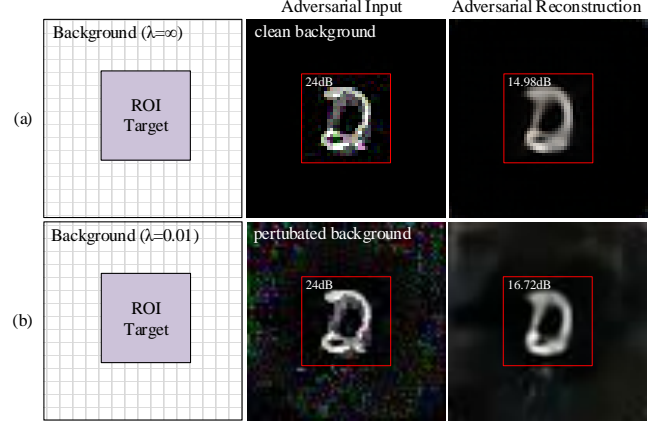


Fig. 23: **Attack with target area mask.** (a) example of adversarial attack with masked ROI (region of interest) target. Zero perturbation is added in the background area. (b) perturbations are added in both the target area and background area with $\lambda = 0.01$ in (16). With same level of target area input perturbation, the attack efficiency is further improved by allowing some extra perturbation in the background area.

difficult to directly apply the (15). For most real-life images, we then suggest a more practical strategy that focuses on alerting salient object or area (e.g. text, face, etc) that is attentive to human observers. The target in an image usually occupies a small fraction of the entire scene, thus we can simply mask out the target area manually or by any target segmentation / saliency detection algorithms while keeping the background unchanged as in Fig. 23(a).

Considering that the stacked convolution layers and resolution resampling used in most NIC solutions would enlarge the receptive field of the network, it implies that the perturbation added in the surrounding background area would also potentially affect the reconstruction of the target area. To fit the general use cases, we still assume that the noise can be added to the entire image, but set different weights in target area \mathbf{x}_{roi} and background area \mathbf{x}_{bkg} in optimization, e.g.,

$$\arg \min_{\mathbf{n}} L_t = \begin{cases} \frac{\|\mathbf{x}_{\text{roi}} - \mathbf{x}_{\text{roi}}^*\|_2^2}{N} + \lambda \frac{\|\mathbf{x}_{\text{bkg}} - \mathbf{x}_{\text{bkg}}^*\|_2^2}{N}, & \frac{\|\mathbf{n}_{\text{roi}}\|_2^2}{N} \geq \epsilon, \\ \frac{\|\hat{\mathbf{x}}_{\text{roi}}^* - \hat{\mathbf{x}}_{\text{roi}}^t\|_2^2}{N} + \lambda \frac{\|\hat{\mathbf{x}}_{\text{bkg}}^* - \hat{\mathbf{x}}_{\text{bkg}}^t\|_2^2}{N}, & \frac{\|\mathbf{n}_{\text{roi}}\|_2^2}{N} < \epsilon. \end{cases} \quad (16)$$

Here the \mathbf{n}_{roi} and ϵ are the noise added in the target area and its threshold. If $\lambda = \infty$ as in Fig. 23(a), Equation (16) is degenerated to (15) that no noise is allowed in the background area. Having a smaller λ that allows some perturbation in the background area can improve the attack efficiency as shown in Fig. 23(b).

2) *Attack Evaluation*: Adversarial examples generated with the optimization function described in (15) on MNIST dataset are shown in Fig. 24. Note that original MNIST dataset are composed of single channel grayscale images. To feed them into image compression models that normally input 3-channel RGB color images, we duplicate them to 3 channels with equal values. Experiment results show that by injecting noise perturbation to input image as in (15), the adversarial

reconstruction significantly differs from the original input and is visually even closer to the designated target. Both MSE and MS-SSIM optimized compression models are vulnerable to such targeted attack.

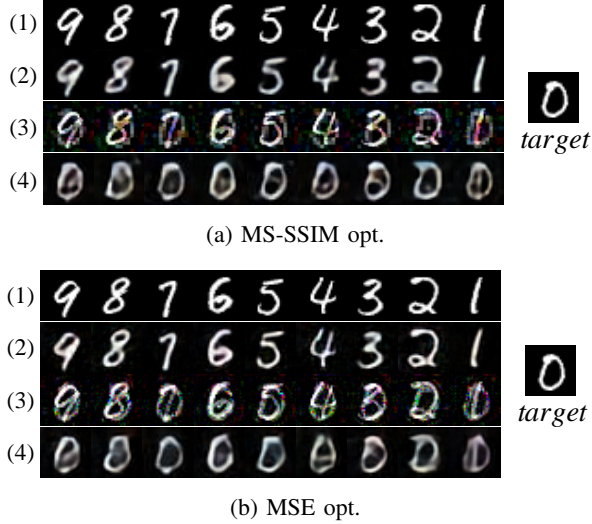


Fig. 24: Targeted adversarial examples and reconstructed output of MNIST [Ref1] samples compressed using (a) MS-SSIM loss optimized Ballé2018 model, and (b) MSE loss optimized Ballé2018 model; (1) original source images, (2) decoded reconstructions of original images, (3) adversarial examples, (4) adversarial reconstructions. The same target image is shown on the right for both MSE and MS-SSIM optimized image compression models.

A high-resolution large-scale dataset Cityscapes [Ref2] that contains a diverse set of stereo videos recorded in street scenes from 50 different cities, is also tested to demonstrate the effectiveness of targeted adversarial attacks with area masking on car plates. We apply (16) to generate targeted adversarial examples where we set $\lambda = 0.1$. As shown in Fig. 25, the numbers in the car plate can be successfully modified to have the adversarial reconstruction closer to the designated target, which may consequently affect the inference engine for decision-making in autonomous driving and surveillance.

3) *Application Limitations:* First, similar to the defense strategy in Sec. V, we can also include targeted adversarial examples into the training stage to finetune the model for improved robustness. However, in real-life applications, the “target” of adversarial attack in pixel domain is abundant, making it impossible to include all potential “targets”. A more practical solution for the defense of targeted attack is to limit the methodology developed in this work to some specific task.

Besides, we mainly focus on pixel-wise attack that affects the reconstruction visually in this paper. Another important domain of adversarial attack is to fool the artificial system (e.g. the accuracy of face recognition system) instead of human eyes. We leave the problem of the defense of targeted attack and the attack of NIC solutions in computer vision tasks for future study.



Fig. 25: Targeted adversarial attack on Cityscapes dataset with plate ROI mask. The license plate number area is marked in red box as the target area.

REFERENCES

- [Ref1] Y. Lecun, L. Bottou, Y. Bengio, and P. Haffner, “Gradient-based learning applied to document recognition,” *Proceedings of the IEEE*, vol. 86, no. 11, pp. 2278–2324, 1998. 19
- [Ref2] M. Cordts, M. Omran, S. Ramos, T. Rehfeld, M. Enzweiler, R. Benenson, U. Franke, S. Roth, and B. Schiele, “The cityscapes dataset for semantic urban scene understanding,” in *Proc. of the IEEE Conference on Computer Vision and Pattern Recognition (CVPR)*, 2016. 19